Globular clusters in the inner Galaxy classified from dynamical orbital criteria

Angeles Pérez-Villegas [ID],[1]* Beatriz Barbuy [ID],[1]* Leandro O. Kerber [ID],[2] Sergio Ortolani [ID],[3] Stefano O. Souza [ID][1] and Eduardo Bica [ID][4]

[1]*Universidade de São Paulo, IAG , Rua do Matão 1226, Cidade Universitária, São Paulo 05508-900, Brazil*
[2]*Universidade Estadual de Santa Cruz, Departamento de Ciências Exatas e Tecnológicas, Rodovia Jorge Amado km 16, Ilhéus 45662-000, Brazil*
[3]*Dipartimento di Fisica e Astronomia 'Galileo Galilei', Università di Padova, Vicolo dell'Osservatorio 3, Padova I-35122, Italy*
[4]*Departamento de Astronomia, Universidade Federal do Rio Grande do Sul, CP 15051, Porto Alegre 91501-970, Brazil*

ABSTRACT

Globular clusters (GCs) are the most ancient stellar systems in the Milky Way. Therefore, they play a key role in the understanding of the early chemical and dynamical evolution of our Galaxy. Around 40 per cent of them are placed within ∼4 kpc from the Galactic centre. In that region, all Galactic components overlap, making their disentanglement a challenging task. With *Gaia* Data Release 2, we have accurate absolute proper motions for the entire sample of known GCs that have been associated with the bulge/bar region. Combining them with distances, from RR Lyrae when available, as well as radial velocities from spectroscopy, we can perform an orbital analysis of the sample, employing a steady Galactic potential with a bar. We applied a clustering algorithm to the orbital parameters apogalactic distance and the maximum vertical excursion from the plane, in order to identify the clusters that have high probability to belong to the bulge/bar, thick disc, inner halo, or outer halo component. We found that ∼ 30 per cent of the clusters classified as bulge GCs based on their location are just passing by the inner Galaxy, they appear to belong to the inner halo or thick disc component, instead. Most GCs that are confirmed to be bulge GCs are not following the bar structure and are older than the epoch of the bar formation.

Key words: Galaxy: bulge – globular clusters: general – Galaxy: kinematics and dynamics.

1 INTRODUCTION

The orbital evolution of globular clusters (GCs) in the Galaxy, combined with kinematics and stellar population analyses, can provide important information to decipher the history of our Galaxy. In Bica, Ortolani & Barbuy (2016), 43 clusters were selected as related to the bulge component based on their location. Recently, Bica et al. (2019) compiled 200 GCs in the Galaxy, adding new entries such as the recently detected ones in the Vista Variables in the Via Lactea (Saito et al. 2012) survey by Minniti, Alonso-García & Pullen (2017a) and Minniti et al. (2017b). By including confirmed GCs plus candidates, the number rises to 294 objects, thus reducing the lack of the Galactic GCs with respect to M31 (Caldwell & Romanowsky 2016).

The stellar population components in the Galaxy have been under scrutiny in the last decades. The Galactic disc and halo are well established, and the existence of a thick disc is increasingly more confirmed. As for the Galactic bulge configuration as an entity, it still

is under definition. In early work, a sample of metal-rich GCs with a flattened distribution were identified as disc GCs by Zinn (1980, 1985). The properties of this disc system of metal-rich GCs were described by Armandroff (1989), to have a scale height between 0.8 and 1.5 kpc, a rotational velocity of $193 \pm 29 \, \mathrm{km \, s^{-1}}$, and a line-of-sight velocity dispersion of $59 \pm 14 \, \mathrm{km \, s^{-1}}$, concluding that these parameters are consistent with properties of thick-disc stars. Later, Frenk & White (1982), Minniti (1995), and Côté (1999) deduced that metal-rich GCs within 3 kpc from the Galactic centre, should be associated with the Galactic bulge rather than to the thick disc, based on kinematics, spatial distribution, and metallicity.

The Galactic bulge formation is under study in several contexts. Barbuy, Chiappini & Gerhard (2018a) list the following possible scenarios: (a) bulge and thick disc were formed early on simultaneously through strong gas accretion, (b) hierarchical merging of subclumps, (c) merging of early thick-disc subclumps, (d) a major merger, (e) secular evolution of the bar, and (f) dwarf galaxies accretion. There is also the hypothesis of the oldest stellar populations in the Galactic bulge to be seen as an extension of the inner halo in the innermost Galaxy.

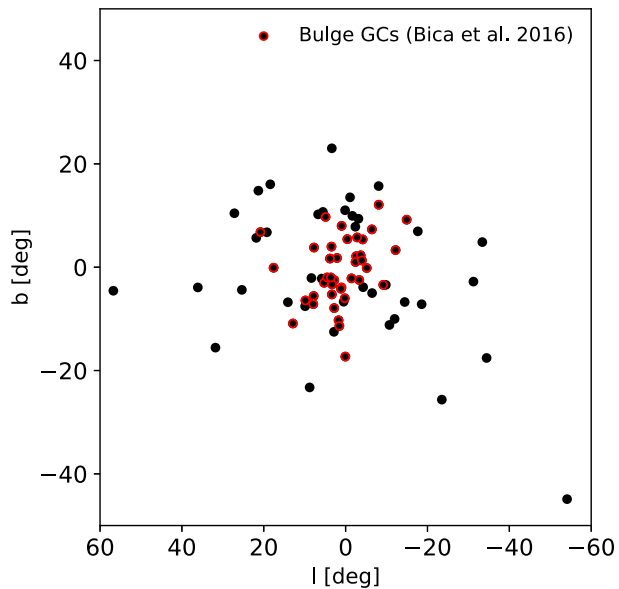* E-mail: mperez@iag.usp.br (AP-V); b.barbuy@iag.usp.br (BB)

Figure 1. Location in Galactic coordinates of the GCs analysed. The red open circles are the clusters classified as bulge GCs in Bica et al. (2016).

The dynamical properties of GCs and their orbits provide further information that would help allocating the objects to a given stellar population. With the recently available *Gaia* Data Release 2 (DR2; Gaia Collaboration 2018a), the investigation of cluster orbits is made timely. Previously, this kind of work was attempted for the bulge clusters, by Dinescu et al. (2003). More recently, Pérez-Villegas et al. (2018) and Rossi et al. (2015b) derived proper motions and orbits for nine inner bulge clusters.

In this work, we study a sample of bulge GCs, plus the intruders or outsiders from Bica et al. (2016, their tables 1 and 2). In order to compute orbits, reliable radial velocities, proper motions, and distances are needed. Radial velocities, which can only be derived from spectroscopy, are still missing for about a dozen of these clusters, making that 78 of them can be studied. The dynamical parameters perigalactic and apogalactic distances, maximum height from the plane and eccentricity, are derived such that their appartenance to different Galaxy components are identified.

In Section 2, the sample and available data are described. In Section 3, the Galactic model potential is detailed. In Section 4, dynamical properties of the orbits are discussed, and in Section 5 the GCs are classified. The bulge GCs are further discussed in Section 6, and conclusions are drawn in Section 7.

2 DATA

The sample includes 40 GCs from the list of bulge GCs by Bica et al. (2016, their table 1), for which radial velocities are available. Another 37 GCs from the outer shell, clusters somewhat farther, at distances $3.0 < d_{GC} < 4.5$ kpc, some clusters with $d_{GC} > 4.5$ kpc from the Galactic centre (Bica et al. 2016; their table 2), and the halo GC NGC 6752 are also added, with the purpose of identifying differences in the orbital properties among clusters that belong to each Galactic component. Fig. 1 shows the location in Galactic coordinates of our total sample that contains 78 clusters.

In Table 1, we list the cluster parameters employed in this study. Equatorial (α, δ) and Galactic (l, b) coordinates are given

in Columns 2–5. The heliocentric distance $d_\odot$, in Column 6 is taken from colour–magnitude diagrams (CMDs) and RR Lyrae star distance determination for the clusters HP 1, Terzan 10, NGC 6522, NGC 6626, NGC 6558, Djorgovski 1, Djorgovski 2, NGC 6304, NGC 6624, NGC 6637, NGC 6652, NGC 6717, NGC 6723, and NGC 6362 (Kerber et al. 2018; Barbuy et al. 2018b; Kerber et al. 2019; Ortolani et al. 2019a,b; Oliveira et al., in preparation) that we consider reliable. For the others, distances from Harris (1996, edition of 2010, hereafter H10), or Baumgardt et al. (2019) were adopted. Radial velocities V_r, given in Column 7, are taken from spectroscopy analyses from the literature. The absolute proper motions (PMs), $\mu_\alpha^* = \mu_\alpha \cos\delta$, μ_δ, in Columns 8 and 9, are the values estimated from the *Gaia* DR2 (Gaia Collaboration 2018b) and for the clusters marked with a star we calculated the PMs following the procedure explained next, where the uncertainties of PMs include the systematic error of 0.035 mas yr^{-1} reported by the Gaia Collaboration (2018b). The metallicties, given in Column 10, available from high-resolution studies reported in Bica et al. (2016, their table 3), Barbuy et al. (2014, 2018b) for NGC 6522 and NGC 6558, derivations from literature and isochrone fittings to CMDs from our group (Oliveira et al., in preparation), and for the remaining clusters the values are adopted from the website by Bruno Dias.[1] Column 11 gives the core radius taken from H10.

For the proper motion derivation from *Gaia* DR2, we selected the individual stars with the astrometric information including positions and PMs within 5 arcmin from the cluster centre. We removed the stars with PM errors > 0.25 mas yr^{-1}. Then, stars in each cluster were retrieved, within the core radius of each cluster from H10 to estimate the PMs. A selection of member stars was carried out with a combined plot of PMs in both directions, and through a Gaussian mixture model (GMM), as shown in Fig. 2, in order to get the mean PM in each direction and their uncertainties. We applied this method to 32 GCs of our sample, and the PM determinations for them are inside 1σ compared with those estimated by Gaia Collaboration (2018b), Vasiliev (2019), and Baumgardt et al. (2019), except for Terzan 1 and Terzan 5, that are inside 3σ. The PMs for the remaining clusters are taken from the new PM determination of GCs using *Gaia* DR2 from the references above.

In the past, the measurement of absolute PMs was a difficult task, particularly for GCs in the innermost Galaxy, and when available, the uncertainties were large, whereas now with *Gaia* that issue is essentially solved. Presently, the input distance values are the major source of uncertainty to construct more precise orbits along the Galaxy, and therefore in the classification of the GCs into a specific stellar population. The distance values for some of them, in particular for the most reddened ones, can be significantly different from H10 or Baumgardt et al. (2019) with their kinematic distance estimations.

Table 2 shows a compilation of distances from the literature. The distances used for the orbital integration are given in column 2, the distances from H10 catalogue are in column 3, the kinematic distances by Baumgardt et al. (2019) in column 4, distance determinations by Valenti, Ferraro & Origlia (2007), Valenti, Ferraro & Origlia (2010) in column 5, the distances estimated by the inverse of the parallax from Gaia Collaboration (2018b) are in column 6, distances taken from isochrone fittings of the CMD and RR Lyrae estimated by our group are given in column

---

[1]http://www.sc.eso.org/~bdias/catalogues.html

Table 1. Globular clusters data.

Cluster	α_{2000} (deg)	δ_{2000} (deg)	l (deg)	b (deg)	$d_\odot$ (kpc)	V_r (km s^{-1})	μ_α^* (mas yr^{-1})	μ_δ (mas yr^{-1})	[Fe/H]† (dex)	$R_c^\ddagger$ (arcmin)
BH 261	273.52	−28.63	3.36	−5.27	6.50 ± 0.65[e]	−29.38 ± 0.60[e]	3.59 ± 0.05	−3.57 ± 0.05	−1.17	0.40
Djorg 1	266.86	−33.06	356.67	−2.48	9.30 ± 0.50[a]	−358.10 ± 0.70[i]	−5.11 ± 0.07	−8.30 ± 0.05	−1.36	0.50
Djorg 2	270.45	−27.82	2.77	−2.50	8.75 ± 0.12[b]	−159.90 ± 0.50[i]	0.58 ± 0.06	−3.05 ± 0.05	−0.91	0.33
ESO452SC11	249.85	−28.39	351.91	12.09	6.50 ± 0.65[e]	16.27 ± 0.48[e]	−1.54 ± 0.05	−6.41 ± 0.05	−1.47	0.50
HP 1*	262.77	−29.98	357.42	2.12	6.59 ± 0.16[c]	40.00 ± 0.50[j]	2.41 ± 0.06	−10.14 ± 0.05	−1.00[m]	0.03
Liller 1	263.35	−33.38	354.84	−0.16	8.20 ± 0.82[d]	60.18 ± 2.46[e]	−5.53 ± 0.52	−7.69 ± 0.33	−0.30[m]	0.06
Lynga 7	242.76	−55.31	328.77	−2.79	8.00 ± 0.80[e]	17.86 ± 0.83[e]	−3.80 ± 0.04	−7.06 ± 0.04	−0.56	0.90
Mercer 5	275.83	−13.66	17.59	−0.11	5.50 ± 0.55[e]	185.50 ± 3.75[e]	−4.22 ± 0.35	−6.97 ± 0.31	−0.85	1.00
NGC 104	6.03	−72.08	305.89	−44.89	4.50 ± 0.45[d]	−48.00 ± 10.00[k]	5.25 ± 0.04	−2.52 ± 0.04	−0.71	0.36
NGC 5927	232.00	−50.68	326.60	4.86	8.16 ± 0.27[e]	−99.00 ± 11.00[e]	−5.05 ± 0.04	−3.23 ± 0.04	−0.32	0.42
NGC 6139	246.92	−38.85	342.36	6.94	9.80 ± 0.83[e]	24.41 ± 0.95[e]	−6.16 ± 0.05	−2.67 ± 0.04	−1.42	0.15
NGC 6144	246.81	−26.02	351.93	15.70	8.90 ± 0.89[d]	195.75 ± 0.74[e]	−1.76 ± 0.04	−2.64 ± 0.04	−2.04	0.94
NGC 6171	248.13	−13.06	3.37	23.01	6.03 ± 0.31[e]	−34.68 ± 0.19[e]	−1.94 ± 0.04	−5.95 ± 0.04	−1.00	0.56
NGC 6235	253.36	−22.17	358.92	13.52	13.52 ± 1.35[e]	126.68 ± 0.33[e]	−3.94 ± 0.04	−7.56 ± 0.04	−1.37	0.33
NGC 6256*	254.88	−37.12	347.79	3.31	6.40 ± 0.64[e]	−103.40 ± 0.50[i]	−3.54 ± 0.05	−1.54 ± 0.05	−1.51	0.02
NGC 6266*	255.31	−30.11	353.58	7.32	6.41 ± 0.12[e]	−73.49 ± 0.70[e]	−5.06 ± 0.07	−2.98 ± 0.07	−1.09	0.22
NGC 6273	255.66	−26.27	356.87	9.38	8.27 ± 0.41[e]	145.54 ± 0.59[e]	−3.22 ± 0.04	1.61 ± 0.04	−1.70	0.43
NGC 6284	256.12	−24.76	358.35	9.94	15.30 ± 1.53[d]	20.70 ± 0.40[i]	−3.19 ± 0.04	−2.05 ± 0.04	−1.07	0.07
NGC 6287	256.29	−22.71	0.13	11.02	9.40 ± 0.94[d]	−294.74 ± 1.65[e]	−4.89 ± 0.04	−1.92 ± 0.04	−2.09	0.29
NGC 6293	257.55	−26.58	357.62	7.83	9.23 ± 0.70[e]	−143.66 ± 0.39[e]	0.82 ± 0.04	−4.31 ± 0.04	−1.92	0.05
NGC 6304*	258.63	−29.46	355.83	5.38	6.28 ± 0.11[f]	−108.62 ± 0.39[e]	−4.01 ± 0.06	−1.03 ± 0.05	−0.45[f]	0.21
NGC 6316*	259.16	−28.14	357.18	5.76	11.60 ± 1.16[e]	92.20 ± 0.60[i]	−4.86 ± 0.06	−4.61 ± 0.06	−0.46	0.17
NGC 6325*	259.50	−23.77	0.97	8.00	7.80 ± 0.78[d]	29.54 ± 0.58[e]	−8.41 ± 0.04	−8.90 ± 0.05	−1.30	0.03
NGC 6333	259.80	−18.52	5.54	10.70	8.40 ± 0.84[e]	310.75 ± 2.12[e]	−2.20 ± 0.04	−3.21 ± 0.04	−1.70	0.45
NGC 6342*	260.29	−19.58	4.90	9.73	8.43 ± 0.84[e]	116.56 ± 0.74[e]	−2.94 ± 0.05	−7.08 ± 0.05	−0.60[m]	0.05
NGC 6352	261.37	−48.43	341.42	−7.17	5.89 ± 0.58[e]	−123.70 ± 0.30[i]	−2.19 ± 0.04	−4.42 ± 0.04	−0.48[f]	0.83
NGC 6355*	260.99	−26.36	359.58	5.43	8.70 ± 0.87[e]	−210.30 ± 0.40[i]	−4.66 ± 0.06	−0.51 ± 0.05	−1.46	0.05
NGC 6356	260.89	−17.82	6.72	10.22	15.10 ± 1.51[d]	38.93 ± 1.88[e]	−3.77 ± 0.04	−3.37 ± 0.04	−0.51	0.24
NGC 6362*	262.97	−67.05	325.55	−17.57	7.69 ± 0.13[f]	−14.58 ± 0.18[e]	−5.47 ± 0.05	−4.72 ± 0.05	−1.07[f]	1.13
NGC 6366	261.93	−5.08	18.41	16.04	3.66 ± 0.20[e]	−118.30 ± 0.30[i]	−0.38 ± 0.04	−5.13 ± 0.04	−0.59	2.17
NGC 6380	263.62	−39.07	350.18	−3.42	9.80 ± 0.98[e]	−6.54 ± 1.48[e]	−2.10 ± 0.04	−3.19 ± 0.04	−0.44	0.34
NGC 6388	264.08	−44.73	345.56	−6.74	10.74 ± 0.12[e]	82.85 ± 0.48[e]	−1.35 ± 0.04	−2.71 ± 0.04	−0.51	0.12
NGC 6401*	264.65	−23.91	3.45	3.98	7.70 ± 0.77[e]	−115.40 ± 0.30[i]	−2.79 ± 0.06	1.49 ± 0.05	−1.08	0.25
NGC 6402	264.39	−3.25	21.32	14.81	9.31 ± 0.44[e]	−60.71 ± 0.45[e]	−3.61 ± 0.04	−5.04 ± 0.04	−1.28	0.79
NGC 6440*	267.22	−20.36	7.73	3.80	8.24 ± 0.82[e]	−54.00 ± 26.00[k]	−1.11 ± 0.07	−3.80 ± 0.07	−0.50[m]	0.14
NGC 6441	267.56	−37.06	353.53	−5.01	11.83 ± 0.14[e]	17.27 ± 0.93[e]	−2.55 ± 0.04	−5.30 ± 0.04	−0.47	0.13
NGC 6453	267.71	−34.60	355.72	−3.87	11.60 ± 1.16[d]	−110.30 ± 0.50[i]	0.07 ± 0.04	−5.85 ± 0.04	−1.55	0.05
NGC 6496	269.76	−44.26	348.03	−10.01	11.30 ± 1.13[d]	−134.72 ± 0.26[e]	−3.03 ± 0.07	−9.20 ± 0.04	−0.60	0.95
NGC 6517	270.47	−8.96	19.23	6.76	10.60 ± 1.06[d]	−65.10 ± 0.20[i]	−1.52 ± 0.04	−4.26 ± 0.04	−1.60	0.06
NGC 6522*	270.89	−30.03	1.02	−3.93	7.40 ± 0.19[g]	−14.40 ± 0.50[l]	2.66 ± 0.06	−6.37 ± 0.06	−0.95[l]	0.05
NGC 6528*	271.20	−30.05	1.14	−4.17	7.70 ± 0.77	185.00 ± 10.00[k]	−2.21 ± 0.07	−5.55 ± 0.07	−0.17[m]	0.13
NGC 6535	270.96	−0.29	27.18	10.44	6.50 ± 0.65[e]	−214.85 ± 0.46[e]	−4.21 ± 0.04	−2.95 ± 0.04	−1.79	0.36
NGC 6539*	271.21	−7.58	20.80	6.78	7.85 ± 0.66[e]	31.30 ± 0.40[i]	−6.89 ± 0.05	−3.54 ± 0.05	−0.79[m]	0.38
NGC 6540*	271.53	−27.76	3.29	−3.31	5.20 ± 0.52[e]	−17.98 ± 0.84[e]	−3.68 ± 0.05	−2.80 ± 0.06	−0.19[m]	0.03
NGC 6541	272.00	−43.71	349.29	−11.18	7.95 ± 0.37[e]	−163.97 ± 0.46[e]	0.28 ± 0.04	−8.77 ± 0.04	−1.80	0.18
NGC 6544	271.83	−24.99	5.84	−2.20	3.00 ± 0.30[d]	−38.12 ± 0.76[e]	−2.33 ± 0.04	−18.56 ± 0.04	−1.37	0.05
NGC 6553	272.32	−25.90	5.25	−3.02	6.75 ± 0.22[e]	0.72 ± 0.40[e]	0.26 ± 0.04	−0.41 ± 0.04	−0.12	0.53
NGC 6558*	272.57	−31.76	0.20	−6.02	8.26 ± 0.53[h]	−194.45 ± 2.10[h]	−1.78 ± 0.04	−4.12 ± 0.04	−1.17[h]	0.03
NGC 6569	273.41	−31.83	0.48	−6.68	10.59 ± 0.80[e]	−49.83 ± 0.50[e]	−4.13 ± 0.04	−7.26 ± 0.04	−0.73	0.35
NGC 6624*	275.92	−30.36	2.79	−7.91	8.43 ± 0.11[f]	54.26 ± 0.45[e]	0.10 ± 0.04	−6.92 ± 0.05	−0.69[f]	0.06
NGC 6626*	276.14	−24.87	7.80	−5.58	5.34 ± 0.17[g]	11.11 ± 0.60[e]	−0.31 ± 0.06	−8.93 ± 0.06	−1.00[m]	0.24
NGC 6637*	277.85	−32.35	1.72	−10.27	8.80 ± 0.88	46.63 ± 1.45[e]	−5.11 ± 0.06	−5.82 ± 0.06	−0.77[m]	0.33
NGC 6638*	277.73	−25.49	7.90	−7.15	10.32 ± 1.03[e]	8.63 ± 2.00[e]	−2.55 ± 0.05	−4.08 ± 0.05	−0.89	0.22
NGC 6642*	277.97	−23.48	9.81	−6.44	8.10 ± 0.81[d]	−33.23 ± 1.13[e]	−0.23 ± 0.05	−3.88 ± 0.05	−1.03	0.10
NGC 6652*	278.94	−32.99	1.53	−11.38	9.51 ± 0.12[f]	−99.04 ± 0.51[e]	−5.47 ± 0.05	−4.20 ± 0.05	−0.85[f]	0.10
NGC 6656	138.69	−49.23	9.89	−7.55	3.20 ± 0.32[d]	−152.00 ± 25.00[k]	9.80 ± 0.04	−5.56 ± 0.04	−1.92	1.33
NGC 6681	283.26	−8.70	2.85	−12.51	9.31 ± 0.17[e]	216.62 ± 0.84[e]	1.39 ± 0.04	−4.72 ± 0.04	−1.55	0.03
NGC 6712	283.27	−8.70	25.35	−4.39	6.95 ± 0.39[e]	−107.45 ± 0.29[e]	3.32 ± 0.04	−4.38 ± 0.04	−0.97	0.76
NGC 6717*	283.78	−22.70	12.88	−10.90	7.14 ± 0.10[f]	32.45 ± 1.44[e]	−3.16 ± 0.05	−4.92 ± 0.05	−1.26[f]	0.08
NGC 6723*	284.89	−36.63	0.07	−17.30	8.17 ± 0.11[f]	−94.18 ± 0.26[e]	0.99 ± 0.05	−2.45 ± 0.05	−1.10[f]	0.83
NGC 6752	287.71	−59.98	336.49	−25.63	4.25 ± 0.09[e]	−26.28 ± 0.16[e]	−3.17 ± 0.04	−4.01 ± 0.04	−1.41	0.17
NGC 6760	287.80	1.03	36.11	−3.92	7.95 ± 0.50[e]	−0.42 ± 1.63[e]	−1.11 ± 0.04	−3.59 ± 0.04	−0.41	0.34
NGC 6809	295.00	−30.97	8.79	−23.27	5.30 ± 0.20[e]	174.40 ± 0.24[e]	−3.40 ± 0.04	−9.26 ± 0.04	−1.87	1.80
NGC 6838	298.44	18.78	56.75	−4.56	4.00 ± 0.20[d]	−42.00 ± 18.00[k]	−3.38 ± 0.04	−2.65 ± 0.04	−0.63	0.63
Palomar 11	296.31	−8.01	31.80	−15.57	14.30 ± 1.40[e]	−67.64 ± 0.76[e]	−1.79 ± 0.05	−4.94 ± 0.05	−0.35	1.19
Palomar 6*	265.93	−26.22	2.10	1.78	5.80 ± 0.58[e]	177.00 ± 1.00[i]	−9.11 ± 0.06	−5.27 ± 0.06	−1.00[m]	0.66
Palomar 7	272.68	−7.20	21.83	5.67	5.39 ± 0.51[e]	155.06 ± 0.69[e]	−2.47 ± 0.05	−4.41 ± 0.05	−0.53	1.01

Table 1 – *continued*

Cluster	α_{2000} (deg)	δ_{2000} (deg)	l (deg)	b (deg)	$d_\odot$ (kpc)	V_r (km s^{-1})	μ_α^* (mas yr^{-1})	μ_δ (mas yr^{-1})	[Fe/H][†] (dex)	$R_c^\ddagger$ (arcmin)
Palomar 8	280.37	− 19.82	14.10	− 6.78	12.80 ± 1.28[e]	− 41.14 ± 1.81[e]	− 2.04 ± 0.04	− 5.64 ± 0.04	− 0.34	0.56
Terzan 1*	263.95	− 30.47	357.57	1.00	6.70 ± 0.67	63.00 ± 0.50[i]	− 3.02 ± 0.05	− 4.49 ± 0.04	− 1.26[m]	0.04
Terzan 10	270.74	− 26.06	4.49	− 1.99	10.40 ± 1.00[a]	208.60 ± 3.20[e]	− 7.02 ± 0.07	− 2.51 ± 0.06	− 0.97	0.90
Terzan 12	273.06	− 22.74	8.36	− 2.10	3.40 ± 0.34[e]	94.77 ± 0.97[e]	− 6.07 ± 0.07	− 2.63 ± 0.07	− 0.47	0.83
Terzan 2*	261.89	− 30.80	356.32	2.30	7.50 ± 0.75[d]	144.60 ± 0.80[d]	− 2.21 ± 0.06	− 6.16 ± 0.05	− 0.42	0.03
Terzan 3*	247.17	− 35.35	345.08	9.19	8.20 ± 0.82[d]	− 135.76 ± 0.57[e]	− 5.61 ± 0.04	− 1.69 ± 0.04	− 0.96	1.18
Terzan 4	262.66	− 31.59	356.02	1.31	6.70 ± 0.67[e]	− 39.93 ± 3.76[e]	− 5.60 ± 0.07	− 2.60 ± 0.12	− 1.60[m]	0.90
Terzan 5*	267.02	− 24.81	3.81	1.67	5.50 ± 0.51[e]	− 81.40 ± 1.36[e]	− 1.35 ± 0.07	− 4.44 ± 0.06	− 0.40	0.16
Terzan 6*	267.69	− 31.28	358.57	− 2.16	6.80 ± 0.68[d]	137.15 ± 1.70[e]	− 5.70 ± 0.11	− 7.20 ± 0.11	− 0.53	0.05
Terzan 9*	270.41	− 26.84	3.61	− 1.99	7.10 ± 0.71[d]	71.40 ± 0.40[i]	− 2.19 ± 0.06	− 7.47 ± 0.05	− 1.08	0.03
Ton 2*	264.04	− 38.55	350.80	− 3.42	6.40 ± 0.64[e]	− 172.70 ± 0.30[i]	− 5.92 ± 0.05	− 0.55 ± 0.05	− 0.26	0.54

Notes. References. [a]Ortolani et al. (2019a) ; [b]Ortolani et al. (2019b); [c]Kerber et al. (2019); [d]Harris (1996, updated in 2010), [e]Baumgardt et al. (2019); [f]Oliveira et al. (2019, in preparation); [g]Kerber et al. (2018); [h]Barbuy et al. (2018b); [i]Vásquez et al. (2018); [j]Barbuy et al. (2016); [k]Dias et al. (2016); [l]Barbuy et al. (2014); [m]Bica et al. (2016, their table 3). [†]Metallicities with no reference come from the website by Bruno Dias (http://www.sc.eso.org/∼bdias/catalogues.html). [‡]R_c taken from H10.
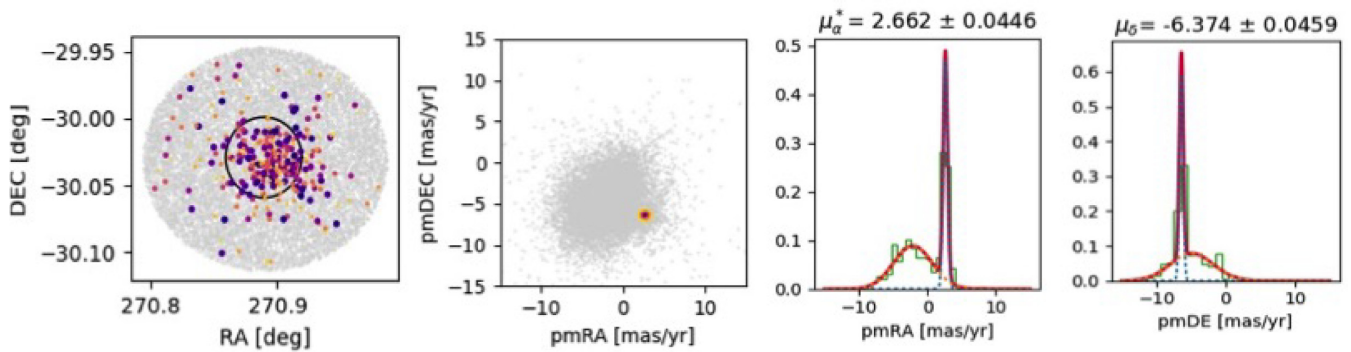

Figure 2. Example of proper motion data from *Gaia* DR2 for NGC 6522, and cluster member selection. First panel: core radius containing the field studied; second panel: location of the cluster in the vector-point diagram; third and fourth panels: Gaussian of RA and Dec. proper motions, respectively.

7, and in column 8 is given the distance compiled by Bica et al. (2006).

The GCs with the largest difference in distance determinations in the literature are Djorg 1, Djorg 2, ESO452SC11, NGC 5927, NGC 6235, NGC 6256, NGC 6316, NGC 6380, NGC 6388, NGC 6401, NGC 6540, NGC 6553, NGC 6638, Palomar 6, Terzan 4, Terzan 5, and Terzan 9.

In order to have a reliable statistical estimate of the uncertainty in distances, we first compared distances from Bica et al. (2006) with those from Valenti et al. (2007, 2010) for 17 bulge clusters in common. These two samples are independent because the first is mostly optical-based and the other is near-infrared-based, with different reddening dependence and different isochrone sets. From the whole sample, we have an uncertainty $\sigma = 1.3$ kpc, but by removing two outliers with errors larger than 2 kpc, which clearly have some specific problems, the uncertainty goes down to $\sigma = 0.99$ kpc. A second check comparing our adopted distances with respect to Baumgardt et al. (2019) and removing two outliers with differences larger than 4 kpc, this results in a standard deviation of 0.4 kpc. From these two comparisons, we adopt a mean standard deviation of 0.7 kpc.

Note that Hilker et al. (2019) report an error on their proper motion distances of 8 per cent at the distance of 7 kpc, which gives an error of 0.6 kpc at the typical distance of the bulge clusters of

7 kpc. This is very consistent with the suggested 0.7 kpc standard deviation.

3 THE GALACTIC POTENTIAL

In order to construct the orbits of the GCs, in this study we employ a non-axisymmetric model for the Galactic gravitational potential, which is built from an axisymmetric background that includes a Sérsic bulge, an exponential disc made by the superposition of three Miyamoto–Nagai potentials (Miyamoto & Nagai 1975), following the recipe given by Smith et al. (2015), and a Navarro–Frenk–White density profile (Navarro, Frenk & White 1997) to model the dark matter halo, having a circular velocity $V_0 = 241$ km s^{-1} at $R_0 = 8.2$ kpc (Bland-Hawthorn & Gerhard 2016). Even though the mass of the dark matter halo is twice larger than usual halo masses of $1.0-1.5 \times 10^{12}$ M$_\odot$, with the scale radius we assumed, the rotation curve inside 30 kpc of our model is in agreement with Bland-Hawthorn & Gerhard (2016), as shown in Fig. 3. We also adopted a less massive DM halo, also reducing the scale radius, and no significant differences are found.

For the Galactic bar, we used a triaxial Ferrer's ellipsoid, where all the mass from the bulge component is converted into a bar. For the bar potential, we consider a total bar mass of 1.2×10^{10} M$_\odot$, an angle of 25° with the Sun-major axis of the bar, a major axis extension of 3.5 kpc, and a gradient of the bar pattern speed values

Table 2. Globular cluster distances from the literature.

Cluster	Adopted (kpc)	H10 (kpc)	Baumgardt + 19 (kpc)	Valenti + 07,10 (kpc)	*Gaia* (1/plx) (kpc)	Our group (kpc)	Bica + 06 (kpc)
BH 261	6.50 ± 0.65	6.50	6.50	–	–	–	–
Djorg 1*	9.30 ± 0.50	13.70	13.70	13.50	–	9.30	8.80
Djorg 2*	8.75 ± 0.20	6.30	6.30	7.0	9.60	8.75	6.70
ESO452SC11*	6.50 ± 0.65	8.30	6.50	–	–	–	7.8
HP 1	6.59 ± 0.16	8.20	6.80	6.80	50.0	6.59	7.40
Liller 1	8.20 ± 0.82	8.20	8.10	7.90	–	7.60	10.50
Lynga 7	8.0 ± 0.80	8.0	8.0	–	–	–	7.2
Mercer 5	5.50 ± 0.55	–	5.50	–	–	–	–
NGC 104	4.50 ± 0.45	4.50	4.43	–	5.10	–	4.50
NGC 5927*	8.16 ± 0.27	7.70	8.16	–	10.04	–	7.60
NGC 6139	9.80 ± 0.83	10.10	9.8	–	–	–	10.1
NGC 6144	8.90 ± 0.89	8.90	8.90	–	14.97	–	10.30
NGC 6171	6.03 ± 0.31	6.40	6.03	–	6.76	–	6.40
NGC 6235*	13.52 ± 1.35	11.50	13.52	–	16.18	–	10.00
NGC 6256*	6.40 ± 0.64	10.30	6.40	9.10	–	6.4	6.60
NGC 6266	6.41 ± 0.12	6.80	6.41	6.6	4.57	–	6.90
NGC 6273	8.27 ± 0.41	8.80	8.27	8.20	10.82	–	8.70
NGC 6284	15.3 ± 1.53	15.3	15.14	–	20.04	–	14.70
NGC 6287	9.40 ± 0.94	9.40	9.40	–	9.31	–	8.50
NGC 6293	9.23 ± 0.70	9.50	9.23	10.50	14.37	–	8.80
NGC 6304	6.28 ± 0.11	5.9	5.77	6.0	9.29	6.19	6.10
NGC 6316*	11.60 ± 1.16	10.40	11.60	11.6	15.17	–	11.00
NGC 6325	7.80 ± 0.78	7.80	7.80	–	6.99	6.90	9.60
NGC 6333	8.40 ± 0.84	7.90	8.40	–	10.70	–	8.20
NGC 6342	8.43 ± 0.84	8.50	8.43	8.40	10.28	–	8.60
NGC 6352	5.89 ± 0.58	5.60	5.89	–	6.48	–	5.70
NGC 6355	8.70 ± 0.87	9.20	8.70	9.0	–	8.80	7.20
NGC 6356	15.10 ± 1.51	15.10	15.10	–	12.64	15	15.20
NGC 6362	7.69 ± 0.13	7.6	7.36	–	10.27	7.71	8.10
NGC 6366	3.66 ± 0.20	3.5	3.66	–	4.36	–	3.60
NGC 6380*	9.80 ± 0.98	10.90	9.80	9.20	9.86	9.8	10.70
NGC 6388*	10.74 ± 0.12	9.90	10.74	11.9	20.74	–	11.50
NGC 6401*	7.7 ± 0.77	10.6	7.7	7.7	8.65	12.0	7.70
NGC 6402	9.31 ± 0.44	9.30	9.31	–	18.66	–	8.90
NGC 6440	8.24 ± 0.82	8.5	8.24	8.20	10.43	8.47	8.40
NGC 6441	11.83 ± 0.14	11.60	11.83	13.5	24.81	–	11.20
NGC 6453	11.60 ± 1.16	11.60	11.60	10.7	23.53	8.5	11.20
NGC 6496	11.30 ± 1.13	11.30	11.30	–	12.45	–	6.60
NGC 6517	10.60 ± 1.06	10.60	10.60	–	46.08	–	10.80
NGC 6522	7.40 ± 0.19	7.70	8	7.40	14.35	7.40	7.80
NGC 6528	7.70 ± 0.77	7.90	7.45	7.50	13.40	7.50	9.10
NGC 6535	6.50 ± 0.65	6.80	6.50	–	7.73	–	6.70
NGC 6539	7.85 ± 0.66	7.8	7.85	8.4	15.87	–	8.40
NGC 6540*	5.20 ± 0.52	5.30	5.20	5.20	–	3.50	3.70
NGC 6541	7.95 ± 0.37	7.5	7.95	–	8.78	–	7.00
NGC 6544	3.0 ± 0.30	3.0	2.60	2.80	3.02	–	2.60
NGC 6553*	6.75 ± 0.22	6.0	6.75	4.90	–	5.20	5.60
NGC 6558	8.26 ± 0.53	7.40	7.20	–	–	8.26	7.40
NGC 6569	10.59 ± 0.80	10.90	10.59	12.0	–	–	8.7
NGC 6624	8.43 ± 0.11	7.9	7.19	8.4	7.26	8.32	8.00
NGC 6626	5.34 ± 0.17	5.5	5.43	–	6.81	5.34	5.70
NGC 6637	8.80 ± 0.88	8.80	8.80	9.40	13.40	8.85	8.60
NGC 6638*	10.32 ± 1.03	9.40	10.32	13.5	–	–	8.40
NGC 6642	8.10 ± 0.81	8.10	8.05	7.0	–	–	7.70
NGC 6652	9.51 ± 0.12	10	10	6.8	9.09	9.44	9.60
NGC 6656	3.20 ± 0.32	3.20	3.23	7.90	3.84	–	3.20
NGC 6681	9.31 ± 0.17	9.0	9.31	–	9.12	–	–
NGC 6712	6.95 ± 0.39	6.90	6.12	–	–	–	6.9
NGC 6717	7.14 ± 0.10	7.10	7.10	–	8.0	7.15	7.40
NGC 6723	8.17 ± 0.11	8.70	8.30	–	13.33	8.05	8.80
NGC 6752	4.25 ± 0.09	4.0	4.25	–	4.32	4.36	4.0
NGC 6760	7.95 ± 0.50	7.40	7.95	–	–	–	7.40
NGC 6809	5.30 ± 0.20	5.40	5.30	–	5.86	–	5.40

Table 2 – *continued*

Cluster	Adopted (kpc)	H10 (kpc)	Baumgardt + 19 (kpc)	Valenti + 07,10 (kpc)	*Gaia* (1/plx) (kpc)	Our group (kpc)	Bica + 06 (kpc)
NGC 6838	4.0 ± 0.20	4.0	3.99	–	4.44	–	3.90
Palomar 11	14.30 ± 1.40	13.4	14.30	–	–	–	12.9
Palomar 6*	5.80 ± 0.58	5.80	5.80	–	–	8.90	7.30
Palomar 7	5.39 ± 0.51	5.40	5.38	–	–	–	5.4
Palomar 8	12.80 ± 1.28	12.80	12.80	–	–	–	12.9
Terzan 1	6.70 ± 0.67	6.70	6.7	9.10	–	5.20	6.20
Terzan 10	10.3 ± 1.0	5.8	5.8	6.6	–	10.30	5.70
Terzan 12	3.40 ± 0.34	4.80	3.40	-	-	-	4.80
Terzan 2	7.50 ± 0.75	7.50	7.50	8.20	–	7.70	8.70
Terzan 3	8.20 ± 0.82	8.20	8.10	–	–	6.50	7.50
Terzan 4*	6.70 ± 0.67	7.20	6.70	–	–	8.0	9.10
Terzan 5*	5.50 ± 0.51	6.90	5.50	10.50	–	5.50	7.60
Terzan 6	6.80 ± 0.68	6.80	6.70	6.0	–	7.0	9.50
Terzan 9*	7.10 ± 0.71	7.10	7.10	11.60	–	4.90	7.70
Ton 2	6.40 ± 0.64	8.20	6.40	–	–	6.40	8.10

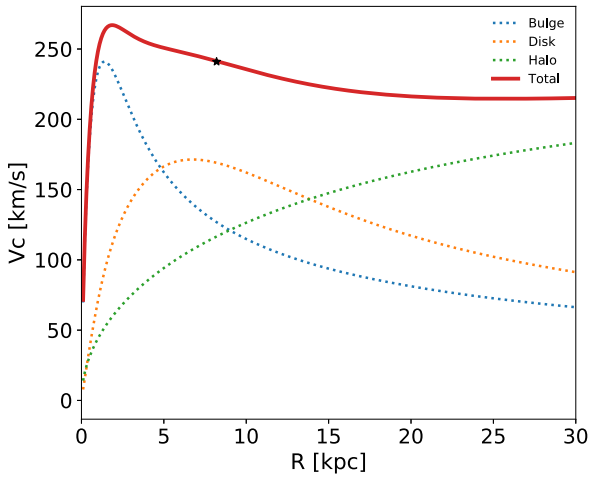*GCs with the largest difference in distance determinations in the literature.

Figure 3. Total circular velocity curve and the contribution of each component of axisymmetric Galactic mass model. The black star shows the velocity at the Sun position.

assumed to be $\Omega_b = 40$, 45, and 50 km s^{-1} kpc^{-1}. We keep the same bar extension in all cases, for any of the bar pattern speed values. Table 3 gives the parameters used for our Galactic model.

4 PROPERTIES OF THE GLOBULAR CLUSTER ORBITS

To construct the GC orbits through the Galactic potential, we have employed the Shampine–Gordon integration scheme that is implemented in the NIGO tool (Numerical Integrator of Galactic Orbits – Rossi 2015a).

We integrated the orbits for the present cluster sample forward in time for 10 Gyr. Using the observational parameters of the GCs given in Table 1, we computed the initial state vector of the clusters assuming the Sun's Galactocentric distance $R_0 = 8.2$ kpc and a circular velocity $V_0 = 241$ km s^{-1} (e.g. Bland-Hawthorn & Gerhard 2016, and references therein). The velocity components of the Sun with respect to the local standard of rest are $(U, V, W)_\odot = (11.1, 12.24, 7.25)$ km s^{-1} (Schönrich, Binney & Dehnen 2010). The velocity components of the cluster in the heliocentric

Table 3. Parameters of the adopted Galactic mass model.

Parameter	Value	Reference
Axisymmetric components		
Bulge		
$M_{b,tot}$	1.2×10^{10} M$_\odot$	1, 2
R_e	0.87 kpc	–
n	1	3
Disc		
$M_{d,1}$	1.07×10^{11} M$_\odot$	–
$a_{d,1}$	5.97 kpc	–
$M_{d,2}$	-7.09×10^{10} M$_\odot$	–
$a_{d,2}$	12.99 kpc	–
$M_{d,3}$	1.2×10^{10} M$_\odot$	–
$a_{d,3}$	2.04 kpc	–
b_d	0.25 kpc	–
Halo		
M_h	3.0×10^{12} M$_\odot$	4
a_h	57.0 kpc	4
Galactic bar		
M_{bar}	1.2×10^{10} M$_\odot$	1, 2, 5
n	2	6
a	3.5 kpc	9, 10
b	1.4 kpc	9, 10
c	1.0 kpc	9, 10
ϕ_{bar}	25°	2, 7, 8
Ω_{bar}	40, 45, 50 km s^{-1} kpc^{-1}	2, 11, 12, 13

Note. References. (1) Portail et al. (2015a); (2) Bland-Hawthorn & Gerhard (2016); (3) Kent et al. (1991); (4) Irrgang et al. (2013); (5) Weiner & Sellwood (1999); (6) Pfenniger (1984); (7) Rattenbury et al. (2007); (8) Wegg & Gerhard (2013); (9) Freudenreich (1998); (10) Gardner & Flynn (2010); (11) Bissantz, Englmaier & Gerhard (2003); (12) Portail et al. (2017); (13) Pérez-Villegas et al. (2017).

reference system $U, V,$ and W are positive in direction of the Galactic centre, Galactic rotation, and North Galactic Pole, respectively. We defined as inertial Galactocentric frame of reference the right-handed system of coordinates (x, y, z), where the x-axis points to the Sun from the Galactic Centre and the z-axis points to the North Galactic Pole. We refer to the bar–corotating frame of reference as the right-handed system of coordinates (x_r, y_r, z_r) that corotates with
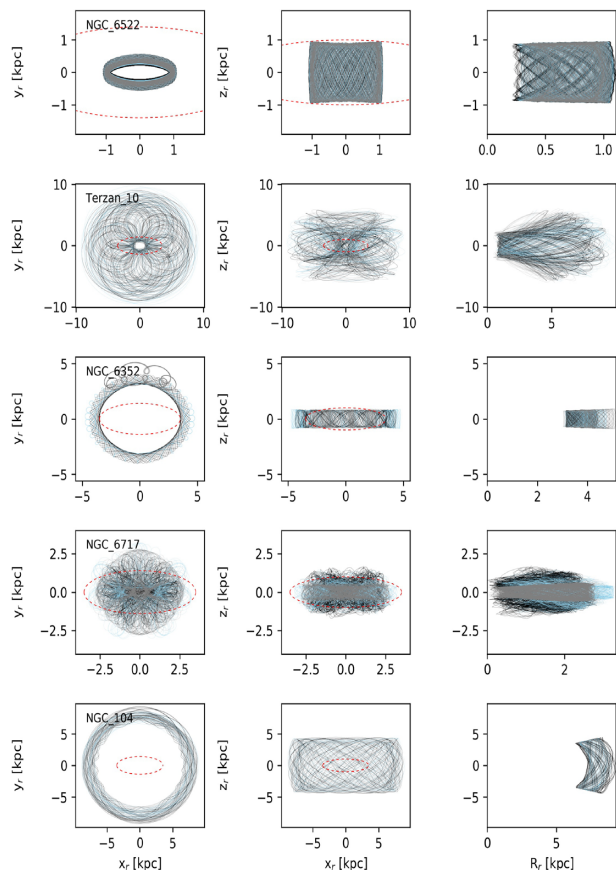
Figure 4. Examples of orbits for the globular clusters. The three columns show x_r-y_r, x_r-z_r, and R_r-z_r projections for orbits with the non-axisymmetric Galactic potential corotating with the bar. The colours in the left-hand panels are the orbits with different pattern speed of the bar, 40 (black), 45 (blue), and 50 (grey) km s^{-1} kpc^{-1}. The dashed red line shows the size of the Galactic bar.

the bar, where the x_r-axis is aligned with the bar semimajor axis a and z_r points towards the north Galactic pole.

For each cluster, we generate a set of 1000 initial conditions, where we follow the Monte Carlo technique taking into account the uncertainties on the heliocentric distance, PMs in both directions, and the radial velocity given in Table 1. The PM uncertainties include the average of the systematic error of 0.035 mas yr^{-1} reported by the Gaia Collaboration (2018b). These calculations were carried out with the purpose of evaluating how much the orbital properties of the GCs change due to the uncertainties of the observed data. Fig. 4 shows some examples of orbits with the three different bar pattern speed values, in the frame corotating with the bar, for five GCs of our sample: NGC 6522, Terzan 10, NGC 6352, NGC 6717, and NGC 104 (from top to bottom). The initial conditions for them are the central values given in Table 1.

The orbital properties we calculate, in the inertial frame of reference, are the perigalactic distance r_{min}, the apogalactic distance r_{max}, the maximum vertical excursion from the Galactic plane $|z|_{max}$, and the eccentricity defined as $e = (r_{max} - r_{min})/(r_{max} + r_{min})$.

In Table 4, we present the orbital parameters of our sample of GCs, where we use three values of rotational velocity of the bar $\Omega_b = 40$, 45, and 50 km s^{-1} kpc^{-1}. For each bar pattern speed, we give the median values of the perigalactic distance $<r_{min}>$,

apogalactic distance $<r_{max}>$, the maximum vertical excursion from the Galactic plane $<|z|_{max}>$, and the orbital eccentricity $<e>$. The errors provided in each column are the standard deviation of the distribution. We see that for the clusters that are confined in the innermost Galaxy, such as HP 1, Djorg 2, Liller 1, and NGC 6325, the effect of the bar pattern speed is almost negligible. On the contrary, for NGC 5927, the perigalactic distance decreases with the pattern speed.

5 CLASSIFYING GLOBULAR CLUSTERS

In the literature, GCs have been classified based on their spatial distribution, metallicity, and internal and structural parameters (e.g. Aguilar, Hut & Ostriker 1988; Minniti 1995; Barbuy, Bica & Ortolani 1998; Côté 1999; Bica et al. 2016; Pasquato & Chung 2019). In this section, we used the orbital parameters of the 78 GCs, calculated in Section 4, to separate the clusters into different stellar populations. We obtained this classification using unsupervised clustering algorithms.

5.1 Clustering method

The identification of GCs that are confined or belong to the bulge/bar component, which is the main aim of this work, is not an easy task because in the innermost part of the Galaxy, all components overlap: the bulge/bar, thick disc, inner halo, and outer halo.

In terms of dynamics, the GCs of each component should share its dynamical properties. Based on this criterion, we employed the orbital parameters (Table 4) to separate the GCs into four Galactic components: bulge/bar, thick disc, inner halo, and outer halo. To do this classification, we employ the GMMs, an unsupervised machine learning algorithm that searches for K Gaussian distributions, which fits better an ND parameter space. Based on Bayes's theorem, the GMM algorithm tries to maximize the expression:

$$G(x) = \sum_{i=1}^{K} \phi_i \times \mathcal{N}(x|\mu_i, \sigma_i),$$

where $\mathcal{N}(x|\mu_i, \sigma_i)$ represents the ith Gaussian distribution with mean μ_i and standard deviation σ_i. The $\vec{x}$ is the parameter space.

We employed the 2D GMM clustering algorithm using two orbital parameters: the apogalactic distance r_{max} and the maximum height from the plane $|z|_{max}$. For the GCs separation, we take into account the contribution of the set of orbits of each GC and the three bar pattern speeds. To prevent confusion in the clustering method, we removed the orbits with $r_{max} > 20$ kpc.

From the GMM algorithm, we obtain the centre $\mu_i(r_{max}, |z|_{max})$, width $\sigma_i(r_{max}, |z|_{max})$, and weight P_i of each stellar component. For the bulge/bar component $\mu_b = (2.50, 1.07)$ kpc, $\sigma_b = (0.83, 0.63)$ kpc, and $P_b = 0.38$; for the thick disc $\mu_d = (5.60, 2.42)$ kpc, $\sigma_d = (1.29, 1.09)$ kpc, and $P_d = 0.46$; for the inner halo $\mu_{H_i} = (8.60, 5.12)$ kpc, $\sigma_{H_i} = (1.31, 1.02)$ kpc, and $P_{H_i} = 0.11$; and outer halo $\mu_{H_o} = (12.75, 8.47)$ kpc, $\sigma_{H_o} = (2.57, 2.18)$ kpc, and $P_{H_o} = 0.032$.

For this work, a statistical approach was necessary since the classification depends on the distribution of the data in the parameter space and their uncertainties. The GMM was applied from the library scikit-learn (Pedregosa et al. 2011).

Table 4. Orbital parameters for different bar pattern speed.

Cluster	$\Omega_b = 40$ km s⁻¹ kpc⁻¹				$\Omega_b = 45$ km s⁻¹ kpc⁻¹				$\Omega_b = 50$ km s⁻¹ kpc⁻¹			
	$\langle r_{min}\rangle$ (kpc)	$\langle r_{max}\rangle$ (kpc)	$\langle |z|_{max}\rangle$ (kpc)	$\langle e\rangle$	$\langle r_{min}\rangle$ (kpc)	$\langle r_{max}\rangle$ (kpc)	$\langle |z|_{max}\rangle$ (kpc)	$\langle e\rangle$	$\langle r_{min}\rangle$ (kpc)	$\langle r_{max}\rangle$ (kpc)	$\langle |z|_{max}\rangle$ (kpc)	$\langle e\rangle$
BH 261	0.47 ± 0.60	3.10 ± 0.57	1.35 ± 0.17	0.74 ± 0.20	0.42 ± 0.53	3.16 ± 0.62	1.34 ± 0.16	0.77 ± 0.17	0.54 ± 0.52	3.22 ± 0.69	1.25 ± 0.15	0.73 ± 0.16
Djorg 1	0.52 ± 0.31	7.02 ± 2.42	3.32 ± 1.16	0.86 ± 0.05	0.47 ± 0.31	7.60 ± 2.59	3.15 ± 1.17	0.87 ± 0.05	0.50 ± 0.32	7.37 ± 2.66	3.09 ± 1.24	0.88 ± 0.05
Djorg 2	0.15 ± 0.12	1.67 ± 0.04	0.55 ± 0.09	0.83 ± 0.11	0.14 ± 0.10	1.66 ± 0.06	0.54 ± 0.16	0.84 ± 0.10	0.09 ± 0.08	1.67 ± 0.11	0.76 ± 0.17	0.91 ± 0.07
ESO452SC11	0.12 ± 0.16	3.45 ± 0.37	2.05 ± 0.12	0.93 ± 0.06	0.12 ± 0.12	3.46 ± 0.42	2.04 ± 0.13	0.93 ± 0.05	0.12 ± 0.14	3.59 ± 0.47	1.99 ± 0.14	0.93 ± 0.05
HP 1	0.12 ± 0.08	3.08 ± 0.37	1.83 ± 0.11	0.93 ± 0.04	0.11 ± 0.07	3.12 ± 0.39	1.84 ± 0.12	0.93 ± 0.04	0.11 ± 0.05	3.00 ± 0.43	1.87 ± 0.12	0.93 ± 0.03
Liller 1	0.08 ± 0.18	1.14 ± 0.41	0.09 ± 0.06	0.88 ± 0.23	0.10 ± 0.18	1.15 ± 0.41	0.09 ± 0.06	0.87 ± 0.23	0.12 ± 0.19	1.13 ± 0.41	0.09 ± 0.06	0.84 ± 0.24
Lynga 7	1.17 ± 0.74	5.27 ± 0.52	1.72 ± 0.25	0.62 ± 0.15	1.73 ± 0.47	5.54 ± 0.63	1.63 ± 0.18	0.53 ± 0.08	1.74 ± 0.37	6.36 ± 0.53	1.45 ± 0.18	0.58 ± 0.08
Mercer 5	1.83 ± 0.20	6.48 ± 1.19	0.17 ± 0.12	0.57 ± 0.06	1.67 ± 0.21	7.83 ± 1.04	0.16 ± 0.11	0.65 ± 0.07	1.47 ± 0.33	7.10 ± 0.45	0.16 ± 0.15	0.66 ± 0.06
NGC 104	7.22 ± 0.12	9.43 ± 0.98	4.47 ± 0.62	0.13 ± 0.05	7.35 ± 0.20	9.24 ± 0.61	4.35 ± 0.49	0.12 ± 0.03	7.37 ± 0.08	9.08 ± 0.82	4.28 ± 0.56	0.10 ± 0.04
NGC 5927	4.20 ± 0.21	6.36 ± 0.23	0.83 ± 0.03	0.21 ± 0.04	3.35 ± 0.35	6.07 ± 0.46	0.81 ± 0.05	0.28 ± 0.07	2.98 ± 0.68	6.11 ± 0.47	0.82 ± 0.05	0.29 ± 0.07
NGC 6139	0.27 ± 0.50	4.50 ± 0.76	2.63 ± 0.31	0.88 ± 0.14	0.21 ± 0.42	4.67 ± 0.80	2.59 ± 0.33	0.90 ± 0.11	0.35 ± 0.46	4.59 ± 0.95	2.55 ± 0.40	0.86 ± 0.13
NGC 6144	0.98 ± 0.69	5.69 ± 1.11	4.61 ± 0.63	0.71 ± 0.21	0.94 ± 0.55	5.84 ± 0.88	4.86 ± 0.81	0.73 ± 0.16	0.77 ± 0.59	5.86 ± 0.81	4.92 ± 0.79	0.78 ± 0.16
NGC 6171	0.58 ± 0.25	5.18 ± 0.42	2.70 ± 0.14	0.81 ± 0.08	0.52 ± 0.23	5.19 ± 0.47	2.67 ± 0.13	0.82 ± 0.07	0.52 ± 0.22	5.04 ± 0.62	2.65 ± 0.15	0.82 ± 0.08
NGC 6235	4.66 ± 1.70	19.73 ± 16.90	10.64 ± 9.66	0.61 ± 0.08	4.68 ± 1.71	19.28 ± 16.88	10.39 ± 9.65	0.61 ± 0.09	4.70 ± 1.69	20.21 ± 16.90	10.83 ± 9.64	0.60 ± 0.08
NGC 6256	2.00 ± 0.83	3.23 ± 0.38	0.61 ± 0.16	0.23 ± 0.22	1.91 ± 0.78	3.25 ± 0.45	0.61 ± 0.16	0.27 ± 0.20	1.52 ± 0.84	3.37 ± 0.61	0.63 ± 0.16	0.36 ± 0.20
NGC 6266	0.32 ± 0.14	2.75 ± 0.16	1.22 ± 0.17	0.80 ± 0.08	0.35 ± 0.16	2.82 ± 0.16	1.10 ± 0.14	0.79 ± 0.09	0.38 ± 0.14	2.93 ± 0.19	1.09 ± 0.08	0.78 ± 0.08
NGC 6273	0.19 ± 0.18	6.25 ± 0.92	4.56 ± 0.60	0.94 ± 0.06	0.20 ± 0.21	6.17 ± 0.96	4.47 ± 0.78	0.94 ± 0.06	0.21 ± 0.20	6.38 ± 0.97	4.82 ± 0.88	0.94 ± 0.06
NGC 6284	0.26 ± 0.94	8.84 ± 1.81	7.34 ± 1.56	0.94 ± 0.12	0.36 ± 0.94	9.78 ± 1.72	7.70 ± 1.52	0.92 ± 0.12	0.33 ± 0.92	9.14 ± 1.87	7.65 ± 1.73	0.92 ± 0.12
NGC 6287	0.18 ± 0.19	8.88 ± 2.06	6.99 ± 2.41	0.96 ± 0.03	0.18 ± 0.21	9.56 ± 2.02	7.31 ± 2.43	0.96 ± 0.03	0.19 ± 0.10	9.51 ± 2.11	7.63 ± 2.42	0.96 ± 0.03
NGC 6293	0.14 ± 0.10	4.38 ± 1.16	2.69 ± 0.64	0.94 ± 0.04	0.15 ± 0.11	4.35 ± 1.16	2.58 ± 0.72	0.94 ± 0.05	0.15 ± 0.10	4.38 ± 1.25	2.52 ± 0.81	0.94 ± 0.04
NGC 6304	0.96 ± 0.19	3.13 ± 0.16	0.91 ± 0.09	0.53 ± 0.07	1.15 ± 0.19	3.16 ± 0.17	0.91 ± 0.07	0.47 ± 0.07	1.18 ± 0.28	3.29 ± 0.28	0.88 ± 0.08	0.48 ± 0.12
NGC 6316	0.71 ± 0.86	4.98 ± 1.76	2.35 ± 0.49	0.76 ± 0.15	0.56 ± 0.89	4.91 ± 1.82	2.41 ± 0.49	0.80 ± 0.15	0.59 ± 0.91	5.01 ± 1.81	2.34 ± 0.49	0.79 ± 0.16
NGC 6325	0.14 ± 0.16	3.46 ± 0.91	2.18 ± 0.32	0.93 ± 0.08	0.14 ± 0.17	3.53 ± 0.90	2.20 ± 0.31	0.92 ± 0.09	0.15 ± 0.18	3.47 ± 1.09	2.23 ± 0.31	0.92 ± 0.10
NGC 6333	0.50 ± 0.23	10.73 ± 1.23	6.29 ± 1.46	0.91 ± 0.04	0.55 ± 0.25	11.06 ± 1.29	6.54 ± 1.41	0.91 ± 0.04	0.55 ± 0.24	11.44 ± 1.68	6.57 ± 1.41	0.91 ± 0.04
NGC 6342	0.14 ± 0.33	3.14 ± 0.68	1.77 ± 0.22	0.91 ± 0.11	0.18 ± 0.34	3.28 ± 0.75	1.72 ± 0.23	0.89 ± 0.12	0.20 ± 0.37	3.32 ± 0.84	1.71 ± 0.25	0.88 ± 0.12
NGC 6352	3.14 ± 0.30	4.43 ± 0.66	0.85 ± 0.06	0.19 ± 0.05	3.12 ± 0.16	4.84 ± 0.84	0.88 ± 0.05	0.22 ± 0.06	3.02 ± 0.14	5.22 ± 0.19	0.90 ± 0.11	0.27 ± 0.03
NGC 6355	0.14 ± 0.14	4.03 ± 1.19	2.48 ± 1.05	0.94 ± 0.05	0.13 ± 0.14	4.16 ± 1.20	2.51 ± 1.04	0.94 ± 0.05	0.14 ± 0.16	4.32 ± 1.28	2.49 ± 1.15	0.94 ± 0.06
NGC 6356	2.46 ± 2.18	9.06 ± 1.78	4.49 ± 1.13	0.58 ± 0.21	2.68 ± 2.21	8.66 ± 1.89	4.60 ± 1.16	0.52 ± 0.22	2.62 ± 2.22	8.83 ± 2.05	4.57 ± 1.16	0.54 ± 0.22
NGC 6362	2.94 ± 0.08	6.64 ± 0.11	3.69 ± 0.05	0.39 ± 0.02	2.81 ± 0.03	5.44 ± 0.03	3.34 ± 0.07	0.32 ± 0.01	1.95 ± 0.05	5.41 ± 0.05	3.33 ± 0.08	0.47 ± 0.01
NGC 6366	1.85 ± 0.29	6.49 ± 0.25	2.40 ± 0.16	0.56 ± 0.05	1.78 ± 0.17	7.26 ± 0.30	2.53 ± 0.29	0.61 ± 0.03	1.44 ± 0.10	6.69 ± 0.10	2.52 ± 0.17	0.64 ± 0.02
NGC 6380	0.13 ± 0.06	2.70 ± 0.92	1.64 ± 0.72	0.92 ± 0.06	0.10 ± 0.05	2.73 ± 1.01	1.65 ± 0.65	0.93 ± 0.04	0.09 ± 0.05	2.89 ± 1.05	1.61 ± 0.64	0.94 ± 0.03
NGC 6388	0.17 ± 0.09	5.96 ± 0.59	3.13 ± 0.65	0.94 ± 0.03	0.64 ± 0.20	7.08 ± 0.42	3.24 ± 0.40	0.84 ± 0.05	0.88 ± 0.10	4.77 ± 0.31	2.05 ± 0.13	0.69 ± 0.04
NGC 6401	0.13 ± 0.24	3.11 ± 0.76	1.64 ± 0.59	0.92 ± 0.09	0.14 ± 0.24	3.16 ± 0.79	1.58 ± 0.57	0.92 ± 0.09	0.15 ± 0.26	3.15 ± 0.92	1.57 ± 0.58	0.91 ± 0.10
NGC 6402	0.16 ± 0.16	5.01 ± 0.49	3.07 ± 0.19	0.94 ± 0.05	0.20 ± 0.19	5.05 ± 0.55	3.02 ± 0.19	0.92 ± 0.06	0.23 ± 0.18	5.14 ± 1.12	2.98 ± 0.20	0.92 ± 0.05
NGC 6440	0.09 ± 0.12	1.52 ± 0.41	0.66 ± 0.34	0.90 ± 0.11	0.09 ± 0.17	1.51 ± 0.41	0.70 ± 0.33	0.90 ± 0.15	0.14 ± 0.15	1.52 ± 0.46	0.69 ± 0.37	0.84 ± 0.14
NGC 6441	0.54 ± 0.23	4.38 ± 0.25	1.92 ± 0.36	0.78 ± 0.09	0.73 ± 0.23	4.56 ± 0.25	1.86 ± 0.27	0.73 ± 0.08	0.45 ± 0.23	4.40 ± 0.44	1.98 ± 0.14	0.82 ± 0.08
NGC 6453	0.24 ± 0.75	5.31 ± 1.79	3.56 ± 1.43	0.90 ± 0.13	0.24 ± 0.78	5.33 ± 2.04	3.51 ± 1.43	0.90 ± 0.13	0.31 ± 0.82	6.32 ± 2.12	3.69 ± 1.43	0.89 ± 0.14
NGC 6496	3.75 ± 1.32	13.99 ± 10.64	5.91 ± 5.49	0.60 ± 0.09	3.91 ± 1.31	13.16 ± 10.63	5.68 ± 5.46	0.61 ± 0.10	3.90 ± 1.27	12.95 ± 10.61	5.67 ± 5.48	0.59 ± 0.10
NGC 6517	0.14 ± 0.11	4.83 ± 0.70	2.96 ± 0.40	0.94 ± 0.03	0.12 ± 0.13	4.87 ± 0.94	2.87 ± 0.40	0.95 ± 0.03	0.12 ± 0.11	4.86 ± 1.15	2.79 ± 0.44	0.95 ± 0.03
NGC 6522	0.23 ± 0.11	1.42 ± 0.10	0.96 ± 0.02	0.72 ± 0.11	0.27 ± 0.13	1.41 ± 0.09	0.95 ± 0.02	0.68 ± 0.12	0.31 ± 0.15	1.40 ± 0.09	0.95 ± 0.02	0.64 ± 0.14
NGC 6528	0.07 ± 0.04	1.77 ± 0.49	0.79 ± 0.27	0.92 ± 0.03	0.08 ± 0.06	1.77 ± 0.51	0.78 ± 0.24	0.91 ± 0.04	0.07 ± 0.06	1.78 ± 0.51	0.78 ± 0.23	0.92 ± 0.05
NGC 6535	0.26 ± 0.40	7.77 ± 1.20	4.06 ± 0.89	0.94 ± 0.13	0.83 ± 0.44	5.41 ± 0.82	2.70 ± 0.73	0.73 ± 0.15	0.88 ± 0.40	5.26 ± 0.68	2.69 ± 0.81	0.71 ± 0.14
NGC 6539	1.56 ± 0.46	3.69 ± 0.58	2.42 ± 0.38	0.38 ± 0.14	1.43 ± 0.61	4.40 ± 0.73	2.46 ± 0.42	0.48 ± 0.19	1.39 ± 0.58	4.81 ± 0.69	2.45 ± 0.52	0.54 ± 0.16
NGC 6540	0.78 ± 0.52	3.24 ± 0.50	0.54 ± 0.16	0.61 ± 0.13	0.75 ± 0.44	3.25 ± 0.52	0.60 ± 0.17	0.62 ± 0.10	0.65 ± 0.40	3.26 ± 0.56	0.59 ± 0.15	0.65 ± 0.10

Table 4 – *continued*

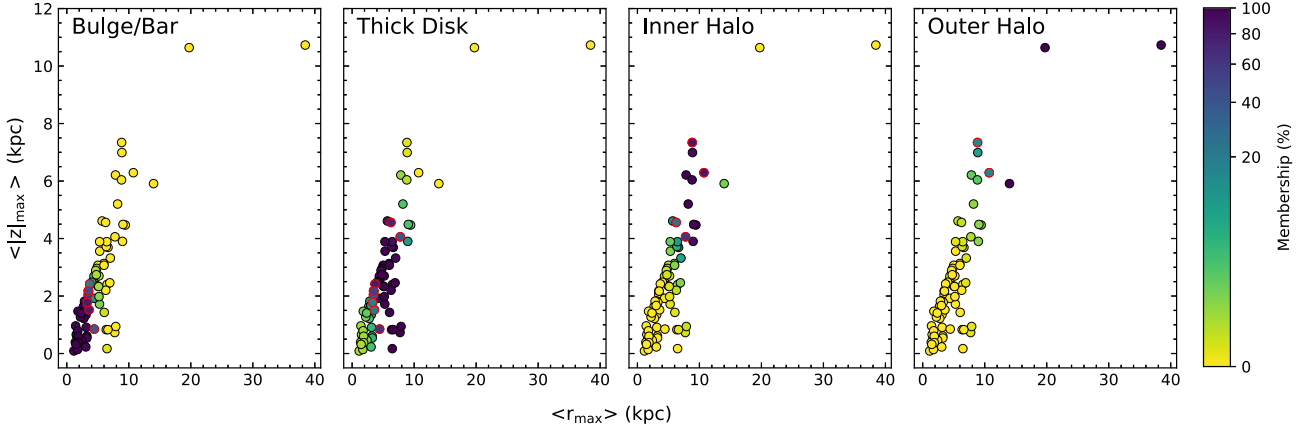| Cluster	$\Omega_b = 40$ km s^{-1} kpc^{-1}				$\Omega_b = 45$ km s^{-1} kpc^{-1}				$\Omega_b = 50$ km s^{-1} kpc^{-1}			
	$<r_{min}>$ (kpc)	$<r_{max}>$ (kpc)	$<\|z\|_{max}>$ (kpc)	$<e>$	$<r_{min}>$ (kpc)	$<r_{max}>$ (kpc)	$<\|z\|_{max}>$ (kpc)	$<e>$	$<r_{min}>$ (kpc)	$<r_{max}>$ (kpc)	$<\|z\|_{max}>$ (kpc)	$<e>$
NGC 6541	0.90 ± 0.36	6.00 ± 0.47	3.07 ± 0.25	0.75 ± 0.10	0.96 ± 0.35	6.37 ± 0.90	3.13 ± 0.37	0.74 ± 0.08	0.97 ± 0.25	7.05 ± 0.60	3.24 ± 0.21	0.76 ± 0.07
NGC 6544	0.17 ± 0.14	6.36 ± 0.53	3.72 ± 0.86	0.95 ± 0.04	0.19 ± 0.14	7.12 ± 0.76	3.75 ± 0.83	0.95 ± 0.04	0.17 ± 0.14	6.37 ± 0.57	3.38 ± 0.65	0.95 ± 0.04
NGC 6553	0.20 ± 0.09	2.40 ± 0.17	0.46 ± 0.03	0.85 ± 0.05	0.29 ± 0.09	2.36 ± 0.17	0.45 ± 0.04	0.78 ± 0.05	0.26 ± 0.14	2.29 ± 0.16	0.44 ± 0.02	0.79 ± 0.07
NGC 6558	0.10 ± 0.07	2.20 ± 0.31	1.27 ± 0.23	0.92 ± 0.05	0.10 ± 0.06	2.19 ± 0.30	1.29 ± 0.23	0.91 ± 0.05	0.09 ± 0.07	2.17 ± 0.33	1.32 ± 0.23	0.92 ± 0.05
NGC 6569	0.42 ± 1.01	3.58 ± 1.12	1.52 ± 0.21	0.79 ± 0.25	0.63 ± 0.91	3.78 ± 1.22	1.48 ± 0.20	0.72 ± 0.21	0.59 ± 0.87	3.71 ± 1.36	1.42 ± 0.19	0.73 ± 0.18
NGC 6624	0.08 ± 0.03	1.80 ± 0.26	1.47 ± 0.04	0.92 ± 0.03	0.08 ± 0.03	1.84 ± 0.18	1.46 ± 0.03	0.92 ± 0.03	0.08 ± 0.03	1.77 ± 0.11	1.46 ± 0.04	0.92 ± 0.03
NGC 6626	0.14 ± 0.09	3.30 ± 0.21	1.78 ± 0.22	0.92 ± 0.05	0.14 ± 0.13	3.32 ± 0.27	1.72 ± 0.19	0.92 ± 0.06	0.13 ± 0.10	3.36 ± 0.33	1.69 ± 0.25	0.92 ± 0.05
NGC 6637	0.12 ± 0.39	2.85 ± 0.72	1.82 ± 0.25	0.92 ± 0.14	0.11 ± 0.44	2.82 ± 0.73	1.82 ± 0.24	0.92 ± 0.17	0.11 ± 0.44	2.87 ± 0.81	1.79 ± 0.25	0.92 ± 0.16
NGC 6638	0.12 ± 0.09	3.51 ± 0.97	2.17 ± 0.48	0.93 ± 0.03	0.11 ± 0.10	3.59 ± 1.05	2.16 ± 0.48	0.94 ± 0.03	0.11 ± 0.10	3.78 ± 1.09	2.13 ± 0.46	0.94 ± 0.03
NGC 6642	0.10 ± 0.09	2.35 ± 0.48	1.41 ± 0.38	0.92 ± 0.06	0.10 ± 0.11	2.24 ± 0.52	1.38 ± 0.41	0.92 ± 0.06	0.09 ± 0.10	2.30 ± 0.58	1.43 ± 0.42	0.93 ± 0.06
NGC 6652	0.13 ± 0.08	4.66 ± 0.54	2.89 ± 0.13	0.94 ± 0.03	0.13 ± 0.10	4.72 ± 0.56	2.91 ± 0.15	0.94 ± 0.04	0.16 ± 0.11	4.82 ± 0.88	2.96 ± 0.17	0.94 ± 0.04
NGC 6656	4.35 ± 0.28	38.45 ± 4.75	10.73 ± 5.56	0.80 ± 0.03	4.33 ± 0.29	38.37 ± 4.76	11.06 ± 5.48	0.80 ± 0.03	4.32 ± 0.28	38.59 ± 4.75	10.72 ± 5.52	0.80 ± 0.03
NGC 6681	0.16 ± 0.07	7.85 ± 0.62	6.21 ± 0.44	0.96 ± 0.02	0.15 ± 0.07	7.99 ± 0.99	6.43 ± 0.48	0.96 ± 0.02	0.16 ± 0.09	8.56 ± 1.03	6.41 ± 0.75	0.96 ± 0.02
NGC 6712	0.37 ± 0.19	6.45 ± 0.86	3.89 ± 0.36	0.90 ± 0.05	0.53 ± 0.25	7.42 ± 0.66	3.61 ± 0.30	0.87 ± 0.06	0.54 ± 0.27	5.94 ± 0.34	2.90 ± 0.50	0.83 ± 0.08
NGC 6717	0.13 ± 0.11	3.02 ± 0.21	1.67 ± 0.14	0.92 ± 0.06	0.27 ± 0.18	3.32 ± 0.23	1.45 ± 0.13	0.85 ± 0.08	0.18 ± 0.15	3.16 ± 0.23	1.46 ± 0.11	0.89 ± 0.07
NGC 6723	0.52 ± 0.32	5.29 ± 0.61	3.89 ± 0.14	0.84 ± 0.10	0.57 ± 0.35	4.82 ± 0.93	3.92 ± 0.16	0.81 ± 0.13	0.23 ± 0.30	4.73 ± 0.95	3.90 ± 0.18	0.91 ± 0.11
NGC 6752	3.25 ± 0.11	6.93 ± 0.12	2.46 ± 0.07	0.36 ± 0.02	2.55 ± 0.14	6.51 ± 0.15	2.34 ± 0.05	0.44 ± 0.03	3.52 ± 0.20	6.38 ± 0.09	2.33 ± 0.05	0.29 ± 0.03
NGC 6760	1.62 ± 0.25	6.04 ± 0.22	1.43 ± 0.57	0.58 ± 0.06	1.51 ± 0.19	6.11 ± 0.53	1.05 ± 0.46	0.60 ± 0.05	1.14 ± 0.22	7.28 ± 0.32	1.10 ± 0.38	0.73 ± 0.05
NGC 6809	0.92 ± 0.24	8.19 ± 0.79	5.20 ± 0.30	0.80 ± 0.05	0.72 ± 0.38	7.62 ± 1.02	4.94 ± 0.29	0.84 ± 0.07	1.05 ± 0.21	8.74 ± 1.12	4.97 ± 0.35	0.78 ± 0.05
NGC 6838	4.75 ± 0.86	7.73 ± 0.14	0.73 ± 0.08	0.24 ± 0.10	4.75 ± 0.69	7.60 ± 0.14	0.72 ± 0.06	0.23 ± 0.07	4.73 ± 0.67	7.68 ± 0.23	0.73 ± 0.06	0.24 ± 0.06
Palomar 11	5.57 ± 2.53	8.98 ± 1.59	3.90 ± 0.62	0.23 ± 0.16	5.67 ± 2.55	8.99 ± 1.56	3.92 ± 0.62	0.25 ± 0.17	5.62 ± 2.49	9.60 ± 1.53	4.12 ± 0.60	0.26 ± 0.17
Palomar 6	0.17 ± 0.20	4.76 ± 1.06	2.74 ± 0.55	0.93 ± 0.06	0.15 ± 0.21	4.71 ± 1.22	2.71 ± 0.55	0.93 ± 0.05	0.17 ± 0.24	4.77 ± 1.53	2.67 ± 0.56	0.93 ± 0.06
Palomar 7	2.86 ± 0.33	7.89 ± 0.90	0.94 ± 0.07	0.47 ± 0.06	2.61 ± 0.62	7.36 ± 0.48	0.88 ± 0.05	0.45 ± 0.07	3.46 ± 0.61	7.10 ± 0.61	0.84 ± 0.05	0.35 ± 0.07
Palomar 8	2.01 ± 1.67	6.28 ± 1.27	2.20 ± 0.21	0.51 ± 0.22	2.03 ± 1.66	6.55 ± 1.21	2.16 ± 0.24	0.55 ± 0.22	1.82 ± 1.67	6.31 ± 1.15	2.22 ± 0.25	0.55 ± 0.22
Terzan 1	0.05 ± 0.05	1.73 ± 0.64	0.14 ± 0.01	0.95 ± 0.06	0.05 ± 0.08	1.70 ± 0.65	0.14 ± 0.02	0.94 ± 0.07	0.04 ± 0.08	1.72 ± 0.66	0.14 ± 0.02	0.95 ± 0.07
Terzan 10	0.57 ± 0.71	8.82 ± 5.04	6.04 ± 4.77	0.87 ± 0.06	0.60 ± 0.71	9.85 ± 5.11	6.11 ± 4.89	0.87 ± 0.06	0.59 ± 0.70	9.43 ± 5.11	6.32 ± 4.83	0.87 ± 0.06
Terzan 12	2.64 ± 0.44	6.63 ± 0.82	0.83 ± 0.09	0.43 ± 0.04	2.19 ± 0.75	7.42 ± 0.65	0.87 ± 0.09	0.46 ± 0.09	3.29 ± 0.78	7.10 ± 0.42	0.85 ± 0.11	0.37 ± 0.10
Terzan 2	0.05 ± 0.03	1.37 ± 0.54	0.39 ± 0.23	0.94 ± 0.03	0.05 ± 0.03	1.35 ± 0.56	0.38 ± 0.23	0.93 ± 0.03	0.06 ± 0.04	1.36 ± 0.57	0.38 ± 0.12	0.93 ± 0.06
Terzan 3	1.32 ± 0.62	5.13 ± 0.61	2.33 ± 0.52	0.62 ± 0.16	1.71 ± 0.35	5.77 ± 0.67	2.21 ± 0.59	0.56 ± 0.09	1.77 ± 0.36	6.18 ± 0.42	2.43 ± 0.46	0.54 ± 0.09
Terzan 4	0.09 ± 0.13	1.86 ± 0.57	0.60 ± 0.15	0.91 ± 0.09	0.11 ± 0.12	1.87 ± 0.57	0.59 ± 0.14	0.89 ± 0.06	0.09 ± 0.15	1.89 ± 0.60	0.59 ± 0.13	0.90 ± 0.07
Terzan 5	0.47 ± 0.26	3.06 ± 0.55	0.23 ± 0.06	0.72 ± 0.06	0.48 ± 0.21	3.04 ± 0.57	0.23 ± 0.06	0.71 ± 0.05	0.54 ± 0.23	3.14 ± 0.61	0.24 ± 0.11	0.70 ± 0.06
Terzan 6	0.06 ± 0.03	1.86 ± 0.72	0.38 ± 0.51	0.94 ± 0.03	0.06 ± 0.03	1.84 ± 0.76	0.39 ± 0.46	0.94 ± 0.03	0.05 ± 0.03	1.83 ± 0.73	0.38 ± 0.46	0.95 ± 0.03
Terzan 9	0.11 ± 0.05	1.46 ± 0.47	0.32 ± 0.06	0.87 ± 0.07	0.10 ± 0.04	1.46 ± 0.47	0.33 ± 0.05	0.88 ± 0.08	0.12 ± 0.06	1.47 ± 0.46	0.33 ± 0.08	0.84 ± 0.09
Ton 2	1.39 ± 0.68	5.19 ± 0.85	1.98 ± 0.18	0.57 ± 0.14	1.75 ± 0.59	5.74 ± 0.85	1.92 ± 0.18	0.54 ± 0.10	1.88 ± 0.48	5.93 ± 0.59	1.91 ± 0.19	0.54 ± 0.10

Figure 5. Membership probability for $\Omega_b = 40\,\mathrm{km\,s^{-1}\,kpc^{-1}}$. From left-hand to right-hand panel shows the probability that each GC has to belong to the bulge/bar, thick disc, inner halo, and outer halo, respectively. The open red circles highlight the clusters with probabilities between 15 per cent and 85 per cent that are in the boundary of two Galactic component.

Table 5. Membership probability for different bar pattern speed.

Cluster	$\Omega_b = 40\,\mathrm{km\,s^{-1}\,kpc^{-1}}$				$\Omega_b = 45\,\mathrm{km\,s^{-1}\,kpc^{-1}}$				$\Omega_b = 50\,\mathrm{km\,s^{-1}\,kpc^{-1}}$			
	Bulge	Disc$_{\mathrm{thick}}$	Halo$_{\mathrm{inner}}$	Halo$_{\mathrm{outer}}$	Bulge	Disc$_{\mathrm{thick}}$	Halo$_{\mathrm{inner}}$	Halo$_{\mathrm{outer}}$	Bulge	Disc$_{\mathrm{thick}}$	Halo$_{\mathrm{inner}}$	Halo$_{\mathrm{outer}}$
			per cent				per cent				per cent	
BH 261	94.2	5.8	0.0	0.0	93.4	6.6	0.0	0.0	93.4	6.6	0.0	0.0
Djorg 1	0.0	93.4	6.6	0.0	0.0	88.7	11.3	0.0	0.0	93.2	6.8	0.0
Djorg 2	99.8	0.2	0.0	0.0	99.8	0.2	0.0	0.0	99.7	0.3	0.0	0.0
ESO452SC11	59.2	40.8	0.0	0.0	59.6	40.4	0.0	0.0	54.3	45.7	0.0	0.0
HP 1	86.5	13.5	0.0	0.0	85.4	14.6	0.0	0.0	87.6	12.4	0.0	0.0
Liller 1	99.8	0.2	0.0	0.0	99.8	0.2	0.0	0.0	99.8	0.2	0.0	0.0
Lynga 7	0.7	99.3	0.0	0.0	0.3	99.7	0.0	0.0	0.0	100.0	0.0	0.0
Mercer 5	0.0	100.0	0.0	0.0	0.0	100.0	0.0	0.0	0.0	100.0	0.0	0.0
NGC 104	0.0	1.2	98.0	0.8	0.0	2.3	97.1	0.6	0.0	3.5	96.0	0.5
NGC 5927	0.0	100.0	0.0	0.0	0.1	99.9	0.0	0.0	0.1	99.9	0.0	0.0
NGC 6139	0.8	99.2	0.0	0.0	0.5	99.4	0.0	0.0	0.8	99.1	0.0	0.0
NGC 6144	0.0	87.1	12.9	0.1	0.0	74.3	25.6	0.1	0.0	71.2	28.7	0.1
NGC 6171	0.0	99.9	0.1	0.0	0.1	99.9	0.1	0.0	0.1	99.9	0.0	0.0
NGC 6235	0.0	0.0	0.0	100.0	0.0	0.0	0.0	100.0	0.0	0.0	0.0	100.0
NGC 6256	96.0	4.0	0.0	0.0	95.9	4.1	0.0	0.0	94.5	5.5	0.0	0.0
NGC 6266	97.7	2.3	0.0	0.0	97.7	2.3	0.0	0.0	97.2	2.8	0.0	0.0
NGC 6273	0.0	73.9	26.1	0.1	0.0	80.3	19.6	0.1	0.0	55.5	44.3	0.1
NGC 6284	0.0	0.0	83.8	16.1	0.0	0.0	46.7	53.3	0.0	0.0	65.4	34.6
NGC 6287	0.0	0.0	91.7	8.3	0.0	0.0	74.7	25.3	0.0	0.0	58.8	41.2
NGC 6293	1.1	98.9	0.0	0.0	1.7	98.2	0.0	0.0	2.0	98.0	0.0	0.0
NGC 6304	96.3	3.7	0.0	0.0	96.0	4.0	0.0	0.0	94.7	5.3	0.0	0.0
NGC 6316	0.4	99.6	0.0	0.0	0.4	99.6	0.0	0.0	0.4	99.6	0.0	0.0
NGC 6325	49.3	50.7	0.0	0.0	43.3	56.7	0.0	0.0	44.7	55.3	0.0	0.0
NGC 6333	0.0	0.0	82.9	17.1	0.0	0.0	64.9	35.1	0.0	0.0	47.8	52.2
NGC 6342	86.6	13.4	0.0	0.0	83.7	16.3	0.0	0.0	82.7	17.3	0.0	0.0
NGC 6352	38.3	61.7	0.0	0.0	11.7	88.3	0.0	0.0	2.8	97.2	0.0	0.0
NGC 6355	6.7	93.3	0.0	0.0	4.1	95.9	0.0	0.0	2.6	97.4	0.0	0.0
NGC 6356	0.0	2.3	97.2	0.6	0.0	3.6	96.0	0.4	0.0	2.8	96.7	0.5
NGC 6362	0.0	91.9	8.1	0.0	0.0	99.5	0.5	0.0	0.0	99.6	0.4	0.0
NGC 6366	0.0	99.7	0.3	0.0	0.0	98.5	1.5	0.0	0.0	99.5	0.5	0.0
NGC 6380	95.8	4.2	0.0	0.0	95.4	4.6	0.0	0.0	94.1	5.9	0.0	0.0
NGC 6388	0.0	99.3	0.7	0.0	0.0	93.9	6.0	0.0	2.1	97.9	0.0	0.0
NGC 6401	90.3	9.7	0.0	0.0	90.1	9.9	0.0	0.0	90.5	9.5	0.0	0.0
NGC 6402	0.0	99.9	0.1	0.0	0.0	99.9	0.1	0.0	0.0	99.9	0.1	0.0
NGC 6440	99.8	0.2	0.0	0.0	99.8	0.2	0.0	0.0	99.8	0.2	0.0	0.0
NGC 6441	11.0	89.0	0.0	0.0	7.0	93.0	0.0	0.0	8.8	91.2	0.0	0.0
NGC 6453	0.0	99.4	0.6	0.0	0.0	99.4	0.6	0.0	0.0	95.2	4.8	0.0
NGC 6496	0.0	0.0	0.9	99.1	0.0	0.0	9.4	90.6	0.0	0.0	14.7	85.3
NGC 6517	0.1	99.9	0.1	0.0	0.1	99.9	0.1	0.0	0.1	99.8	0.0	0.0
NGC 6522	99.8	0.2	0.0	0.0	99.8	0.2	0.0	0.0	99.8	0.2	0.0	0.0
NGC 6528	99.7	0.3	0.0	0.0	99.7	0.3	0.0	0.0	99.7	0.3	0.0	0.0
NGC 6535	0.0	38.9	60.9	0.2	0.0	99.9	0.1	0.0	0.0	99.9	0.1	0.0

Table 5 – *continued*

| Cluster | $\Omega_b = 40 \text{ km s}^{-1} \text{ kpc}^{-1}$ | | | | $\Omega_b = 45 \text{ km s}^{-1} \text{ kpc}^{-1}$ | | | | $\Omega_b = 50 \text{ km s}^{-1} \text{ kpc}^{-1}$ | | | |
| | Bulge | Disc$_{\text{thick}}$ | Halo$_{\text{inner}}$ | Halo$_{\text{outer}}$ | Bulge | Disc$_{\text{thick}}$ | Halo$_{\text{inner}}$ | Halo$_{\text{outer}}$ | Bulge | Disc$_{\text{thick}}$ | Halo$_{\text{inner}}$ | Halo$_{\text{outer}}$ |
		per cent				per cent				per cent		
NGC 6539	19.5	80.5	0.0	0.0	2.2	97.8	0.0	0.0	0.5	99.5	0.0	0.0
NGC 6540	96.1	3.9	0.0	0.0	95.9	4.1	0.0	0.0	95.8	4.2	0.0	0.0
NGC 6541	0.0	99.4	0.6	0.0	0.0	98.6	1.4	0.0	0.0	94.2	5.7	0.0
NGC 6544	0.0	94.6	5.4	0.0	0.0	80.7	19.3	0.1	0.0	97.4	2.6	0.0
NGC 6553	99.3	0.7	0.0	0.0	99.4	0.6	0.0	0.0	99.4	0.6	0.0	0.0
NGC 6558	99.1	0.9	0.0	0.0	99.1	0.9	0.0	0.0	99.1	0.9	0.0	0.0
NGC 6569	78.0	22.0	0.0	0.0	68.5	31.5	0.0	0.0	74.6	25.4	0.0	0.0
NGC 6624	99.3	0.7	0.0	0.0	99.3	0.7	0.0	0.0	99.3	0.7	0.0	0.0
NGC 6626	81.1	18.9	0.0	0.0	82.4	17.6	0.0	0.0	81.8	18.2	0.0	0.0
NGC 6637	91.7	8.3	0.0	0.0	92.2	7.8	0.0	0.0	91.8	8.2	0.0	0.0
NGC 6638	46.7	53.3	0.0	0.0	42.3	57.7	0.0	0.0	32.1	67.9	0.0	0.0
NGC 6642	98.5	1.5	0.0	0.0	98.8	1.2	0.0	0.0	98.6	1.4	0.0	0.0
NGC 6652	0.2	99.8	0.0	0.0	0.1	99.8	0.0	0.0	0.1	99.9	0.1	0.0
NGC 6656	0.0	0.0	0.0	100.0	0.0	0.0	0.0	100.0	0.0	0.0	0.0	100.0
NGC 6681	0.0	0.4	98.3	1.3	0.0	0.2	97.9	1.9	0.0	0.1	97.5	2.4
NGC 6712	0.0	90.8	9.2	0.0	0.0	77.7	22.2	0.1	0.0	99.6	0.4	0.0
NGC 6717	91.4	8.6	0.0	0.0	88.9	11.1	0.0	0.0	92.1	7.9	0.0	0.0
NGC 6723	0.0	98.6	1.4	0.0	0.0	99.4	0.6	0.0	0.0	99.5	0.5	0.0
NGC 6752	0.0	99.3	0.7	0.0	0.0	99.8	0.2	0.0	0.0	99.8	0.2	0.0
NGC 6760	0.0	100.0	0.0	0.0	0.0	99.9	0.0	0.0	0.0	100.0	0.0	0.0
NGC 6809	0.0	2.1	97.4	0.5	0.0	9.6	90.1	0.3	0.0	1.3	98.1	0.5
NGC 6838	0.0	100.0	0.0	0.0	0.0	100.0	0.0	0.0	0.0	100.0	0.0	0.0
Palomar 11	0.0	9.6	89.9	0.5	0.0	9.1	90.4	0.5	0.0	2.0	97.1	0.9
Palomar 6	0.2	99.8	0.0	0.0	0.3	99.7	0.0	0.0	0.3	99.7	0.0	0.0
Palomar 7	0.0	99.9	0.1	0.0	0.0	100.0	0.0	0.0	0.0	100.0	0.0	0.0
Palomar 8	0.0	99.9	0.1	0.0	0.0	99.8	0.2	0.0	0.0	99.9	0.1	0.0
Terzan 1	99.7	0.3	0.0	0.0	99.7	0.3	0.0	0.0	99.7	0.3	0.0	0.0
Terzan 10	0.0	0.1	98.2	1.7	0.0	0.0	95.3	4.7	0.0	0.0	95.9	4.1
Terzan 12	0.0	100.0	0.0	0.0	0.0	100.0	0.0	0.0	0.0	100.0	0.0	0.0
Terzan 2	99.8	0.2	0.0	0.0	99.8	0.2	0.0	0.0	99.8	0.2	0.0	0.0
Terzan 3	0.2	99.8	0.0	0.0	0.0	99.9	0.0	0.0	0.0	99.8	0.2	0.0
Terzan 4	99.7	0.3	0.0	0.0	99.7	0.3	0.0	0.0	99.7	0.3	0.0	0.0
Terzan 5	97.4	2.6	0.0	0.0	97.5	2.5	0.0	0.0	96.9	3.1	0.0	0.0
Terzan 6	99.7	0.3	0.0	0.0	99.7	0.3	0.0	0.0	99.7	0.3	0.0	0.0
Terzan 9	99.8	0.2	0.0	0.0	99.8	0.2	0.0	0.0	99.8	0.2	0.0	0.0
Ton 2	0.5	99.5	0.0	0.0	0.1	99.9	0.0	0.0	0.0	99.9	0.0	0.0

5.2 Membership probability and GC classification

With the information of the each component provided by the GMM and using a Gaussian distribution probability, we calculate the membership probability that each cluster has to belong to each Galactic component. Fig. 5 shows the membership probability for $\Omega_b = 40 \text{ km s}^{-1} \text{ kpc}^{-1}$. The dark blue colour indicates the clusters that have probability higher than 85 per cent to belong to the bulge/bar (first panel), thick disc (second panel), inner halo (third panel), and outer halo (four panel) component. The red open circles mark the clusters with probability between 15 per cent and 85 per cent, that are in the boundary between two Galactic components. Table 5 gives the probability for each cluster to be part of the bulge/bar, disc, inner halo, and outer halo, for the three pattern speeds of the bar.

The maximum probability of membership given in Table 5 was used to classify the GCs into each Galactic component. Fig. 6 shows a plot of combinations among the orbital parameters, where the colours identify the groups of clusters based on the membership probability. Fig. 6 also shows a clear correlation between $<r_{\max}>$ and $<|z|_{\max}>$, and an anticorrelation between $<r_{\min}>$ and eccentricity.

In Table 6, we list the GCs that belong to each of the Galactic components. From our sample has 40 of 43 GCs identified as bulge

GCs in Bica et al. (2016), and based on their dynamical properties, for the pattern speed of $40 \text{ km s}^{-1} \text{ kpc}^{-1}$, we found that 27 of them have characteristics of bulge GCs with a higher probability, whereas the other 13 GCs (Mercer 5, NGC 6316, NGC 6325, NGC 6355, NGC 6539, NGC 6638, NGC 6652, Ton 2, Palomar 6, Djorg 1, Terzan 3, Terzan 10, and NGC 6723) appear to be intruders from other stellar components, which currently are crossing the central parts of the Galaxy, provided that their distances are confirmed in the future. Additionally, the clusters NGC 6380 and NGC 6569 are part of the bulge GCs in our clasification, therefore we have 29 bulge GCs. Another 37, 9, and 3 GCs are identified as thick disc, inner halo, and outer halo, respectively. There are three clusters, NGC 6535, NGC 6284, and NGC 6333, that change component membership with the bar pattern speed. Additionally, there are clusters with significant probability to be in two stellar components. ESO452SC11, NGC 6325, NGC 6352, NGC 6539, NGC 6569, NGC 6626, and NGC 6638 are in the boundary between bulge/bar and thick disc; NGC 6273 and NGC 6535 are between thick disc and inner halo; NGC 6284 and NGC 6333 are between inner halo and outer halo, and these clusters could change with the bar pattern speed. It is important to stress that due to the uncertainties of the data, in particular in the distances, the classification established here, might change in the future when better distance determinations are available. One example is Palomar 6, that with the distance of $d_\odot$
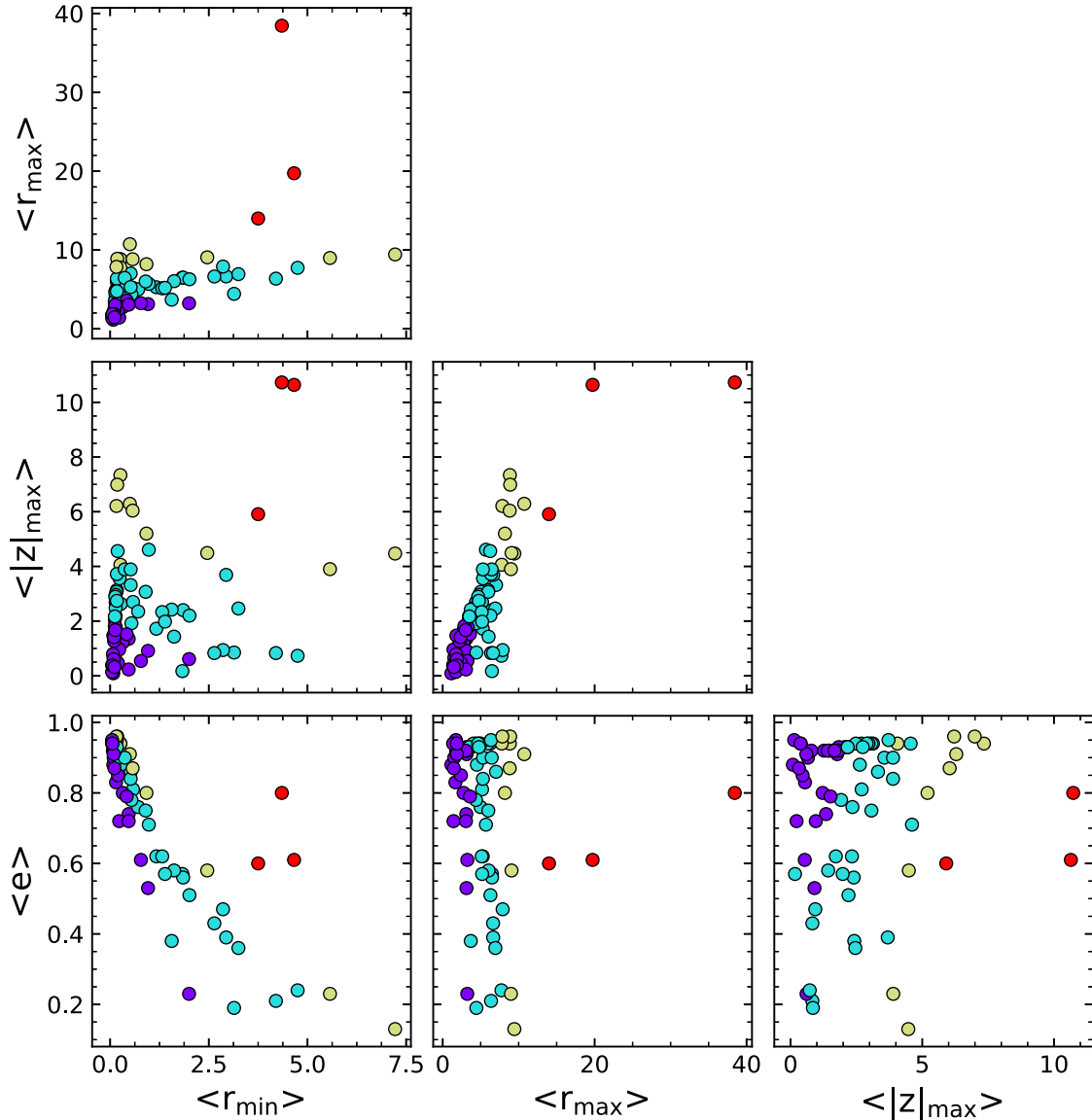
Figure 6. Orbital parameters as function of the median values of the perigalactic distance $<r_{min}>$, the apogalctic ditance $<r_{max}>$, the maximum distance from the Galactic plane $<|z|_{max}>$, and eccentricity $<e>$, for $\Omega_b = 40 \, \mathrm{km \, s^{-1} \, kpc^{-1}}$. The four groups are bulge/bar (purple), thick disc (cyan), inner halo (green), and outer halo (red).

= 5.8 kpc puts it in the thick disc component, whereas the distance by Ortolani, Bica & Barbuy (1995) of $d_\odot = 8.9$ kpc puts it in the bulge.

Fig. 7 shows the spatial distribution of the sample GCs, based on our classification and the stellar component with higher membership probability, where we can note that GCs from different Galactic components overlap in the innermost part of the Galaxy.

6 BULGE GLOBULAR CLUSTERS

Once, we identify clusters with high probability to be bulge GCs, we analyse their set of orbits, with the purpose of knowing which bulge GCs follow the bar. To classify orbits, we use the same criteria defined by Portail, Wegg & Gerhard (2015b). The orbit

classification employs frequency analysis. First, we compute the fast Fourier transform for each orbit in the Cartesian x-coordinate and the Cylindrical radius R, to identify the main frequencies. Then, the orbits for which the frequency ratio $f_R/f_x = 2 \pm 0.1$ are bar-following orbits. The orbits that are not supporting the bar shape have a frequency ratio $f_R/f_x \neq 2 \pm 0.1$. Table 7 gives the percentage of orbits in each bulge GC that support the bar shape. The clusters Liller 1, NGC 6304, NGC 6522, NGC 6528, NGC 6540, NGC 6553, Terzan 5, and Terzan 9 have more than 20 per cent of their orbits that support the bar. The fraction of orbits that follow the Galactic bar decreases with the rotation of the bar, except for the cases of NGC 6304, NGC 6342, and NGC 6637, which increases instead. Also, we found that most of the bulge/bar GCs are not suporting the Galactic bar.

On the other hand, there are bulge GCs that even if they are not supporting the bar shape, they are trapped into a bar

Table 6. Classification of GCs based on dynamical properties, assuming their maximum membership probability.

Component	Clusters		
Bulge/Bar	BH 261	NGC 6401	NGC 6637
	Djorg 2	NGC 6440	NGC 6642
	ESO452SC11	NGC 6522	NGC 6717
	HP 1	NGC 6528	Terzan 1
	Liller 1	NGC 6540	Terzan 2
	NGC 6256	NGC 6553	Terzan 4
	NGC 6266	NGC 6558	Terzan 5
	NGC 6304	NGC 6569	Terzan 6
	NGC 6342	NGC 6624	Terzan 9
	NGC 6380	NGC 6626	
Thick disc	Djorg 1	NGC 6388	NGC 6712
	Lynga 7	NGC 6362	NGC 6723
	Mercer 5	NGC 6366	NGC 6752
	NGC 5927	NGC 6402	NGC 6760
	NGC 6139	NGC 6441	NGC 6838
	NGC 6144	NGC 6453	Palomar 6
	NGC 6171	NGC 6517	Palomar 7
	NGC 6273	NGC 6535*	Palomar 8
	NGC 6293	NGC 6539	Terzan 12
	NGC 6316	NGC 6541	Terzan 3
	NGC 6325	NGC 6544	Ton 2
	NGC 6352	NGC 6638	
	NGC 6355	NGC 6652	
Inner halo	NGC 104	NGC 6356	Palomar 11
	NGC 6284*	NGC 6681	Terzan 10
	NGC 6287	NGC 6809	NGC 6333*
Outer halo	NGC 6235	NGC 6496	NGC 6656

*GCs that its classification changes with Ω_b.

resonance such as NGC 6266 and NGC 6558, in the 3:1 resonance.

Additionally, the metallicity distribution function of the classified bulge GCs is shown in Fig. 8, where we can note a clear peak at [Fe/H] ~ -1.0, as previously already reported by Rossi et al.

Table 7. Bulge GC orbits that follow the Galactic bar for different pattern speed.

Cluster	Orbits following the bar (per cent)		
	$\Omega_b = 40$	$\Omega_b = 45$	$\Omega_b = 50$
BH 261	6.2	6.9	8.9
Djorg 2	0.0	0.1	0.0
ESO452SC11	0.0	0.2	0.0
HP 1	0.2	0.4	0.8
Liller 1	38.2	32.1	28.1
NGC 6256	9.0	19.7	36.1
NGC 6266	13.1	9.9	8.3
NGC 6304	27.8	38.1	38.4
NGC 6342	1.0	3.1	3.5
NGC 6380	0.7	0.9	0.3
NGC 6401	0.7	0.7	1.4
NGC 6440	11.3	9.1	7.5
NGC 6522	97.0	95.3	94.7
NGC 6528	44.0	24.0	7.8
NGC 6540	23.1	18.2	12.9
NGC 6553	65.2	63.3	57.0
NGC 6558	19.3	12.5	6.9
NGC 6569	2.0	2.6	3.1
NGC 6624	0.3	0.0	0.1
NGC 6626	0.4	0.1	0.5
NGC 6637	1.3	4.2	4.4
NGC 6642	7.2	2.8	2.1
NGC 6717	0.7	0.8	0.7
Terzan 1	2.0	2.3	1.6
Terzan 2	0.0	0.0	0.0
Terzan 4	19.6	15.1	13.7
Terzan 5	32.8	25.0	12.3
Terzan 6	1.7	2.1	0.5
Terzan 9	87.7	81.8	73.1

(2015b) and Bica et al. (2016). Fig. 9 gives the metallicity as a function of the median value of the orbital parameters, the perigalactic and apogalactic distances, the maximum height, and the eccentricity. We cannot see any trend among orbital parameters
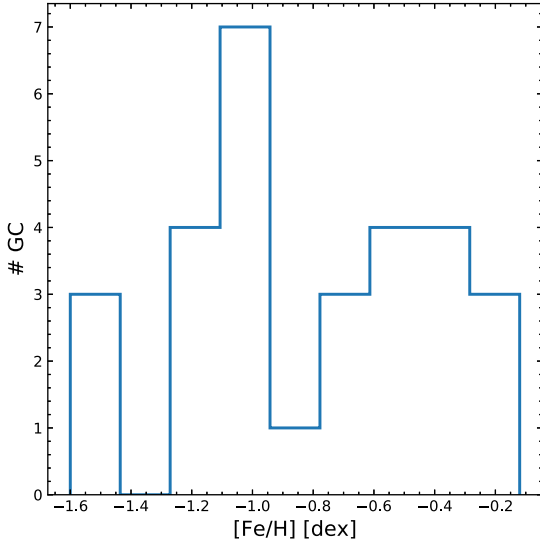
Figure 7. Spatial distribution of the GCs in the $x-y$ (left-hand panel) and $x-z$ (right-hand planel) projection. The colours are the same as in Fig. 6 and indicate the stellar component to which GCs are associated. The black dashed line shows the size of the Galactic bar.

Figure 8. Metallicity distribution of bulge globular clusters.

with the metallicity. Also, the effect of changing the bar pattern speed is almost negligible for the bulge GCs.

7 CONCLUSIONS

Combining accurate absolute PMs from *Gaia* DR2 with distances from RR Lyrae and/or CMD when available, and radial velocities from spectroscopy, we were able to construct the orbits of 78 GCs among the most centrally located in the Galaxy, using a Galactic bar potential. Most sample clusters are located in the innermost region of the MW.

We generate a set of initial conditions for each cluster using Monte Carlo simulations, taking into account the uncertainties from the heliocentric distance and kinematic data of the clusters. We calculated the median value of the orbital parameters such as the perigalactic and apogalactic distances, the maximum vertical excursion from the Galactic plane, and the eccentricity. Through the dynamical properties of the orbits, apogalactic distance, and the maximum height from the plane, we applied a clustering technique to estimate the membership probability that each cluster has to be part of different stellar populations: bulge/bar, thick disc, inner halo, or outer halo.

Given that in the inner part of the MW, most of Galactic components overlap, one of the goals of this study was to identify which among the bulge GCs classified as such by Bica et al. (2016), are confined in the bulge/bar region. In a few cases, like Djorg 1 and Terzan 10, they are identified as halo intruders in the Galactic bulge (Ortolani et al. 2019a), and with our analysis, we confirm that they are in fact contaminating the bulge GC population. Others in the same case are NGC 6316, NGC 6355, Ton 2, Palomar 6, and NGC 6723, provided that their distances are confirmed. In terms of dynamical properties, the orbital characteristics of the GCs identified to be part of the bulge/bar are distinct from those in the thick disc/inner halo according to the present classification criteria.

The GCs are very old, whereas the bar likely formed later. In the already seminal paper by Sheth et al. (2008), it was shown that whereas 65 per cent of the present-day luminous spiral galaxies have bars, at redshift $z \sim 0.84$ (about 6 Gyr ago), this fraction drops to 20 per cent at redshift $z = 0$. From a fully cosmological simulation, Buck et al. (2018) suggest that the Galaxy's bar formed 8 ± 2 Gyr ago. Similarly, Bovy et al. (2019) used chemical abundances from the *Apache Point Observatory Galactic Evolution Experiment* survey, and kinematical information from the Gaia collaboration, and concluded that the Galactic bar formed ~ 8 Gyr ago. Therefore, the fact that GCs are in the bar, probably indicates that they were confined in the bar when the latter formed.

Most of the bulge GCs are confined in the bar region but are not supporting the bar structure, and the seven clusters that are supporting the bar do not necessarily support the X-shape. In particular, Terzan 5, which is confined in the bar, was revealed to have multiple populations in a range of metallicities and ages (Origlia et al. 2019, and references therein), suggesting this object to be the nucleus of a dwarf galaxy.

Currently, we have very accurate proper motions from *Gaia* and radial velocities from high-resolution spectroscopy, however, in most cases there are no accurate distance determinations, and they are crucial to characterize the orbits. Further efforts on distance derivation from accurate CMDs and/or RR Lyrae, are greatly needed.
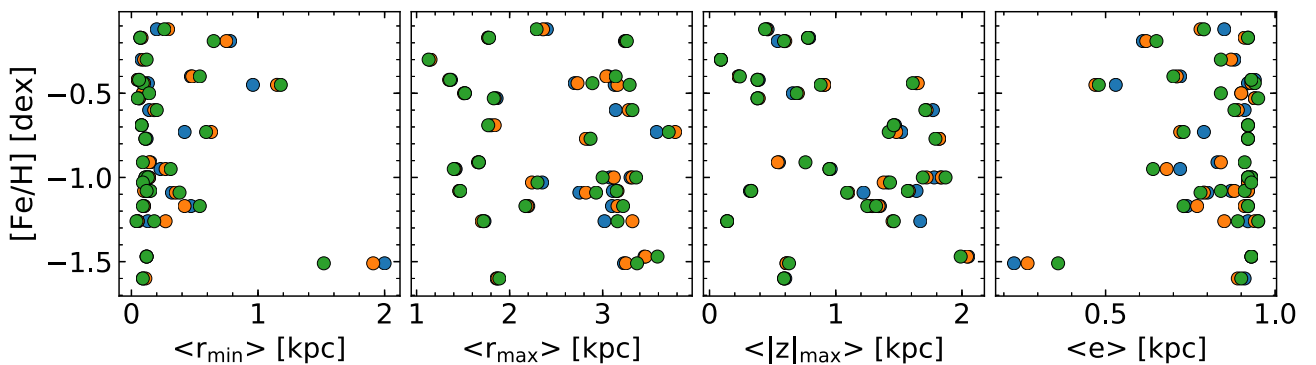
Figure 9. Metallicity of bulge globular clusters as a function of the median values of perigalactic distance $<r_{min}>$ (first panel), apogalactic distance $<r_{max}>$ (second panel), maximum distance from the Galactic plane $<|z|_{max}>$ (third panel), and eccentricity $<e>$ (fourth panel), for $\Omega_b = 40$ (blue), 45 (orange), and 50 (green) km s^{-1} kpc^{-1}.

REFERENCES

Aguilar L., Hut P., Ostriker J. P., 1988, ApJ, 335, 720
Armandroff T. E., 1989, AJ, 97, 375
Barbuy B., Bica E., Ortolani S., 1998, A&A, 333, 117
Barbuy B., et al., 2014, A&A, 570, A76
Barbuy B., et al., 2016, A&A, 591, A53
Barbuy B., Chiappini C., Gerhard O., 2018a, ARA&A, 56, 223
Barbuy B., et al., 2018b, A&A, 619, A178
Baumgardt H., Hilker M., Sollima A., Bellini A., 2019, MNRAS, 482, 5138
Bica E., Bonatto C., Barbuy B., Ortolani S., 2006, A&A, 450, 105
Bica E., Ortolani S., Barbuy B., 2016, Publ. Astron. Soc. Aust., 33, e028
Bica E., Pavani D. B., Bonatto C. J., Lima E. F., 2019, AJ, 157, 12
Bissantz N., Englmaier P., Gerhard O., 2003, MNRAS, 340, 949
Bland-Hawthorn J., Gerhard O., 2016, ARA&A, 54, 529
Bovy J., Leung H. W., Hunt J. A. S., Mackereth J. T., García-Hernández D. A., Roman-Lopes A., 2019, MNRAS, 490, 740
Buck T., Ness M. K., Obreja A., Maccio A. V., Dutton A. A., 2018, ApJ, 861, 88
Caldwell N., Romanowsky A. J., 2016, ApJ, 824, 42
Côté P., 1999, AJ, 118, 406
Dias B., Barbuy B., Saviane I., Held E. V., Da Costa G. S., Ortolani S., Gullieuszik M., Vásquez S., 2016, A&A, 590, A9
Dinescu D. I., Girard T. M., van Altena W. F., López C. E., 2003, AJ, 125, 1373
Frenk C., White S., 1982, MNRAS, 198, 173
Freudenreich H. T., 1998, ApJ, 492, 495
Gaia Collaboration, 2018a, A&A, 616, A1
Gaia Collaboration, 2018b, A&A, 616, A12
Gardner E., Flynn C., 2010, MNRAS, 405, 545
Harris W. E., 1996, AJ, 112, 1487
Hilker M., Baumgardt H., Sollima A., Bellini A., 2019, preprint (arXiv: 1908.02778)

Irrgang A., Wilcox B., Tucker E., Schiefelbein L., 2013, A&A, 549, A137
Kent S. M., Dame T. M., Fazio G., 1991, ApJ, 378, 131
Kerber L. O., Nardiello D., Ortolani S., Barbuy B., Bica E., Cassisi S., Libralato M., Vieira R. G., 2018, ApJ, 853, 15
Kerber L. O. et al., 2019, MNRAS, 484, 5530
Minniti D., 1995, AJ, 109, 1663
Minniti D., Alonso-García J., Pullen J., 2017a, Res. Notes Am. Astron. Soc., 1, 54
Minniti D. et al., 2017b, ApJ, 849, L24
Miyamoto M., Nagai R., 1975, PASJ, 27, 533
Navarro J. F., Frenk C. S., White S. D. M., 1997, ApJ, 490, 493
Origlia L. et al., 2019, ApJ, 871, 114
Ortolani S., Bica E., Barbuy B., 1995, A&A, 296, 680
Ortolani S., Nardiello D., Pérez-Villegas A., Bica E., Barbuy B., 2019a, A&A, 622, A94
Ortolani S. et al., 2019b, A&A, 627, A145
Pasquato M., Chung C., 2019, MNRAS, 490, 3392
Pedregosa F., Varoquaux G., Gramfort A. et al., 2011, JMLR, 12, 2825
Pérez-Villegas A., Portail M., Wegg C., Gerhard O., 2017, ApJ, 840, L2
Pérez-Villegas A., Rossi L., Ortolani S., Casotto S., Barbuy B., Bica E., 2018, Publ. Astron. Soc. Aust., 35, e021
Pfenniger D., 1984, A&A, 134, 373
Portail M., Wegg C., Gerhard O., Martinez-Valpuesta I., 2015a, MNRAS, 448, 713
Portail M., Wegg C., Gerhard O., 2015b, MNRAS, 450, L66
Portail M., Gerhard O., Wegg C., Ness M., 2017, MNRAS, 465, 1621
Rattenbury N. J., Mao S., Sumi T., Smith M. C., 2007, MNRAS, 378, 1064
Rossi L. J., 2015a, Astron. Comput., 12, 11
Rossi L. J., Ortolani S., Barbuy B., Bica E., Bonfanti A., 2015b, MNRAS, 450, 3270
Saito R. K. et al., 2012, A&A, 537, A107
Schönrich R., Binney J., Dehnen W., 2010, MNRAS, 403, 1829
Sheth K. et al., 2008, ApJ, 675, 1141
Smith R., Flynn C., Candlish G. N., Fellhauer M., Gibson B. K., 2015, MNRAS, 448, 2934
Valenti E., Ferraro F. R., Origlia L., 2007, AJ, 133, 1287
Valenti E., Ferraro F. R., Origlia L., 2010, MNRAS, 402, 1729
Vasiliev E., 2019, MNRAS, 484, 2832
Vásquez S. et al., 2018, A&A, 619, A13
Wegg C., Gerhard O., 2013, MNRAS, 435, 1874
Weiner B. J., Sellwood J. A., 1999, ApJ, 524, 112
Zinn R., 1980, ApJ, 241, 602
Zinn R., 1985, ApJ, 293, 424

This paper has been typeset from a TEX/LATEX file prepared by the author.